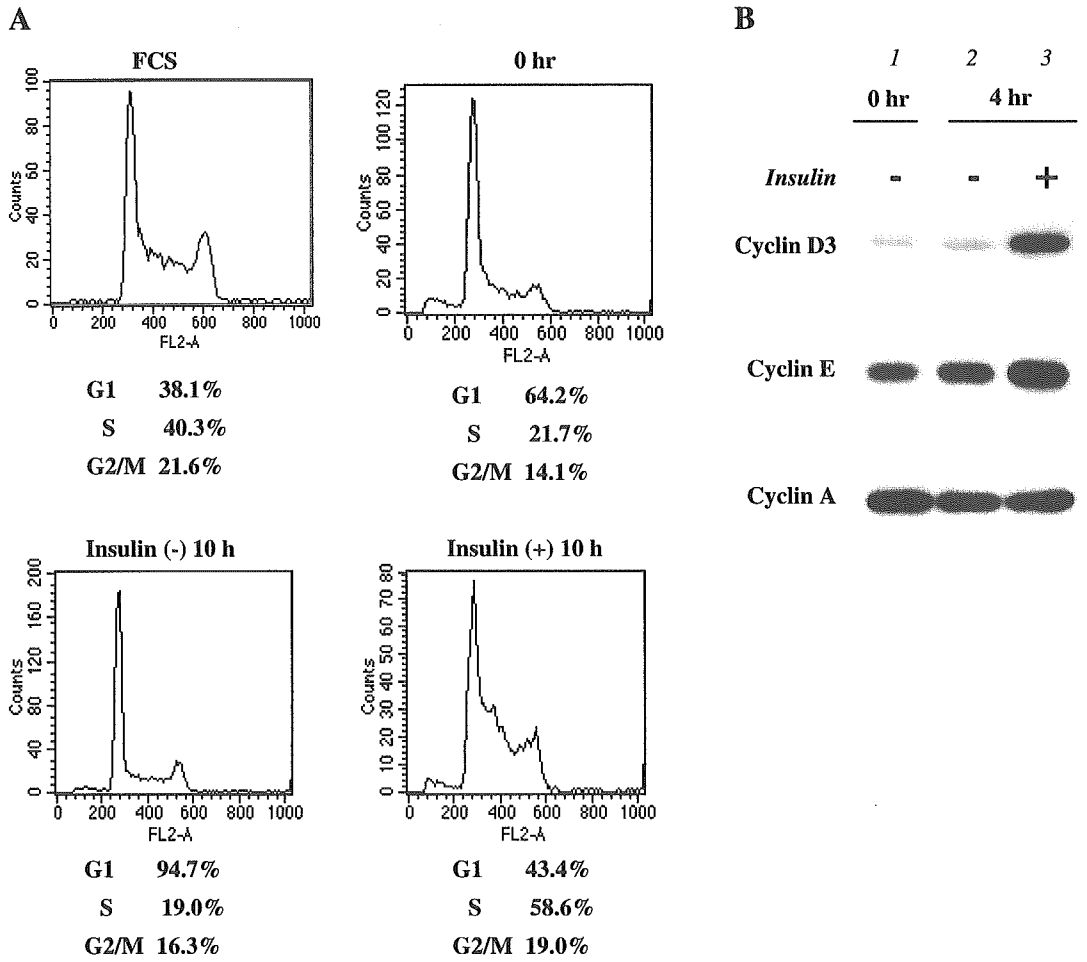

Fig. 9. Cell cycle analysis and expressions of cyclins. *A*: cells cultured with transferrin-supplemented serum-free medium for 3 days were stimulated with buffer solution (*bottom left*) or insulin (*bottom right*). After another 10-h incubation at 37°C, cells were fixed with 70% ethanol and subjected to DNA content assessment by fluorescence-activated cell sorting. Cells cultured in the presence of serum were also subjected to flow cytometric analysis (*top left*). *B*: cells cultured with transferrin-supplemented serum-free medium for 3 days were stimulated with buffer solution (*lane 2*) or insulin (*lane 3*). Cell lysates were prepared after another 4-h incubation. Western blotting was performed using anti-cyclin D3, followed by anti-cyclin E and anti-cyclin A reblotting.

sion was observed 4 h after stimulation (Fig. 8*A*, *lane 4*). Because serum stimulation activates SRp20 transcription and increases the protein expression of SRp20 as the cells enter into S-phase (9), the recovery in SRp2 expression would be associated with the cell cycling progression. As shown in Fig. 9, the insulin treatment significantly increased the S-phased population. Thus the recovery in SRp20 in later phases is associated with an enhanced S-entry.

Thus insulin treatment causes qualitative changes of CLIC1 that are associated with its subnuclear localization and the proteasome-dependent degradations of SRp20 as early as 1 h.

DISCUSSION

We identified CLIC1 and SRp20 as novel downstream effectors of insulin-dependent signals in human hematopoietic cells by using a 2-DE-based proteome analytic system.

A 2-DE-based proteome analysis has merit in managing a wide spectrum of protein expressions atone time. Moreover, it can illustrate the change in modifications and subcellular localization of the proteins besides the change in net amounts. As in the case of CLIC1, glyceraldehyde-3-phosphate dehydrogenase (GAPDH) expressions in 2-DE were upregulated by insulin stimulation, although no significant changes were detected in 1-DE (K. Saeki, unpublished observation). Because serum stimulation, which often induces similar protein expression changes as insulin stimulation, reportedly induces cytoplasmic transport of GAPDH (18), the upregulated expression of GAPDH in 2-DE may be associated with similar subcellular translocation.

Although CLIC1 functions as a chloride ion channel when localized to membranes (26), it is known that CLIC1 localizes principally to the cell nucleus in human hematopoietic cells (24). CLIC1 is structurally homologous to the GST superfamily of proteins with a redox-active site at the NH_2 terminus (5). It is suggested that CLICL1 activity is under the control of redox-active signaling molecules in vivo (5). In this sense, it is interesting that GST-pi is also a downstream effector of insulin as we showed (Fig. 1*A*, *spot c*) and reported elsewhere (6). It is known that hyperglycemia and, to a lesser extent, insulin resistance cause oxidative stress (15, 13). Insulin signaling might possibly contribute to the reduction of oxidative stresses by changing the expression patterns of CLICL1 and GST-pi. Further investigations are required to understand the molecular basis and biological relevance of insulin-induced changes in CLIC1 in the 2-DE system.

As for *spots d* and *e* of SRp20, we could not find any differences in PMFs. One interpretation is that distinct phosphorylations took place at their COOH-terminal SR domains. Because the SR domain is extremely rich in arginine residues, this domain should be degraded into pieces after trypsin digestion, and, as a result, the peptide fragment ions might be hardly detectable. In any case, the expressions of *spots d* and *e* were both decreased by insulin stimulation, and thus the precise determination of structural differences between the two spots would be a less important subject for an understanding of biological effects of insulin. As we showed, the insulin-induced reduction in SRp20 was inhibited by pretreatment of the cells by MG-132, a reversible proteasome inhibitor (Fig. 8*B*). Quite unexpectedly, lactacystin, an irreversible proteasome inhibitor, could not inhibit the reduction of SRp20, although it effectively enhanced an insulin-dependent accumulation of cyclin D3 (K. Saeki, unpublished observation), suggesting that there might be at least two different proteasome-dependent protein degradation systems with distinct lactacystin susceptibilities.

What is the impact of SRp20 reduction by insulin? SRp20 is a splicing factor involved in the regulation of alternative splicing of certain precursor RNA, including SRp20 itself. Its roles for embryogenesis have been shown: an inactivation of SRp20 gene in mice resulted in a failure to form blastocysts, and embryos died at morula stage (11). Although complete loss of SRp20 functions is toxic, its mild reduction may play roles in particular situations. It is reported that overexpression of ASF/SF2, an alternative splicing regulator that antagonizes the function of SRp20 (10), was detected in malignant ovarian tissues (4). A transient reduction of SRp20 by insulin might upregulate the activity of ASF/SF2 and thus trigger signals for cell proliferation. Further investigations are required to determine the in vivo significance of a transient reduction of SRp20 after insulin stimulation.

ACKNOWLEDGMENTS

We greatly thank Masaki Yamada and Tsutomu Nishine of Shimadzu Corporation for technical assistance with the amino acid sequence analysis performed using an MS/MS and PSD mode of MALDI-TOF-MS (AXIMA-QIT and AXIMA-CFRplus).

GRANTS

This work was supported, in part, by a grant for diabetes research (MF-4) from the Organization for Pharmaceutical Safety and Research (to Y. Kaburagi).

REFERENCES

1. **Araki E, Lipes MA, Patti ME, Bruning JC, Haag B III, Johnson RS, and Kahn CR.** Alternative pathway of insulin signalling in mice with targeted disruption of the IRS-1 gene. *Nature* 372: 186–190, 1994.
2. **Blommaart EF, Luiken JJ, Blommaart PJ, van Woerkom GM, and Meijer AJ.** Phosphorylation of ribosomal protein S6 is inhibitory for autophagy in isolated rat hepatocytes. *J Biol Chem* 270: 2320–2326, 1995.
3. **Edvardsson U, Alexandersson M, Brockenhuus von Lowenhielm H., Nystrom AC, Ljung B, Nilsson F, and Dahllof B.** A proteome analysis of livers from obese (ob/ob) mice treated with the peroxisome proliferator WY14,643. *Electrophoresis* 20: 935–942, 1999.
4. **Fischer DC, Noack K, Runnebaum IB, Watermann DO, Kieback DG, Stamm S, and Stickeler E.** Expression of splicing factors in human ovarian cancer. *Oncol Rep* 11: 1085–1090, 2004.
5. **Harrop SJ, DeMaere MZ, Fairlie WD, Reztsova T, Valenzuela SM, Mazzanti M, Tonini R, Qiu MR, Jankova L, Warton K, Bauskin AR, Wu WM, Pankhurst S, Campbell TJ, Breit SN, and Curmi PM.** Crystal structure of a soluble form of the intracellular chloride ion channel CLIC1 (NCC27) at 1.4-A resolution. *J Biol Chem* 276: 44993–5000, 2001.
6. **Hatayama I, Yamada Y, Tanaka K, Ichihara A, and Sato K.** Induction of glutathione S-transferase P-form in primary cultured rat hepatocytes by epidermal growth factor and insulin. *Jpn J Cancer Res* 82: 807–814, 1991.
7. **Jaleel A and Nair KS.** Identification of multiple proteins whose synthetic rates are enhanced by high amino acid levels in rat hepatocytes. *Am J Physiol Endocrinol Metab* 286: E950–E957, 2004.
8. **Joshi RL, Lamothe B, Cordonnier N, Mesbah K, Monthioux E, Jami J, and Bucchini D.** Targeted disruption of the insulin receptor gene in the mouse results in neonatal lethality. *EMBO J* 15: 1542–1547, 1996.
9. **Jumaa H, Guenet JL, and Nielsen P.** Regulated expression and RNA processing of transcripts from the Srp20 splicing factor gene during the cell cycle. *Mol Cell Biol* 17: 3116–3124, 1997.
10. **Jumaa H and Nielsen PJ.** The splicing factor SRp20 modifies splicing of its own mRNA and ASF/SF2 antagonizes this regulation. *EMBO J* 16: 5077–5085, 1997.
11. **Jumaa H, Wei G, and Nielsen PJ.** Blastocyst formation is blocked in mouse embryos lacking the splicing factor SRp20. *Curr Biol* 9: 899–902, 1999.
12. **Kaburagi Y, Yamauchi T, Yamamoto-Honda R, Ueki K, Tobe K, Akanuma Y, Yazaki Y, and Kadowaki T.** The mechanism of insulin-induced signal transduction mediated by the insulin receptor substrate family. *Endocr J* 46, *Suppl*: S25–S34, 1999.
13. **King GL and Loeken MR.** Hyperglycemia-induced oxidative stress in diabetic complications. *Histochem Cell Biol* 122: 333–338, 2004.
14. **Liu JP, Baker J, Perkins AS, Robertson EJ, and Efstratiadis A.** Mice carrying null mutations of the genes encoding insulin-like growth factor 1 (Igf-1) and type 1 IGF receptor (Igf1r). *Cell* 75: 59–72, 1993.
15. **Robertson RP.** Chronic oxidative stress as a central mechanism for glucose toxicity in pancreatic islet beta cells in diabetes. *J Biol Chem* 279: 42351–42354, 2004.
16. **Saeki K, Hong Z, Nakatsu M, Yoshimori T, Kabeya Y, Yamamoto A, Kaburagi Y, and Yuo A.** Insulin-dependent signaling regulates azurophil granule-selective macroautophagy in human myeloblastic cells. *J Leukoc Biol* 74: 1108–1116, 2003.
17. **Sasaoka T and Kobayashi M.** The functional significance of Shc in insulin signaling as a substrate of the insulin receptor. *Endocr J* 47: 373–381, 2000.
18. **Schmitz HD.** Reversible nuclear translocation of glyceraldehyde-3-phosphate dehydrogenase upon serum depletion. *Eur J Cell Biol* 80: 419–427, 2001.
19. **Shisheva A, Buxton J, and Czech MP.** Differential intracellular localizations of GDP dissociation inhibitor isoforms. Insulin-dependent redistribution of GDP dissociation inhibitor-2 in 3T3-L1 adipocytes. *J Biol Chem* 269: 23865–32868, 1994.
20. **Sun XJ, Rothenberg P, Kahn CR, Backer JM, Araki E, Wilden PA, Cahill DA, Goldstein BJ, and White MF.** Structure of the insulin receptor substrate IRS-1 defines a unique signal transduction protein. *Nature* 352: 73–77, 1991.
21. **Sun XJ, Wang LM, Zhang Y, Yenush L, Myers MG Jr, Glasheen E, Lane WS, Pierce JH, and White MF.** Role of IRS-2 in insulin and cytokine signalling. *Nature* 377: 173–177, 1995.
22. **Tobe K, Tamemoto H, Yamauchi T, Aizawa S, Yazaki Y, and Kadowaki T.** Identification of a 190-kDa protein as a novel substrate for the insulin receptor kinase functionally similar to insulin receptor substrate-1. *J Biol Chem* 270: 5698–5701, 1995.
23. **Toda T, Sugimoto M, Omori A, Matsuzaki T, Furuichi Y, and Kimura N.** Proteomic analysis of Epstein-Barr virus-transformed human B-lymphoblastoid cell lines before and after immortalization. *Electrophoresis* 21: 1814–1822, 2000.
24. **Valentinis B, Romano G, Peruzzi F, Morrione A, Prisco M, Soddu S, Cristofanelli B, Sacchi A, and Baserga R.** Growth and differentiation signals by the insulin-like growth factor 1 receptor in hemopoietic cells are mediated through different pathways. *J Biol Chem* 274: 12423–12430, 1999.
25. **Valenzuela SM, Martin DK, Por SB, Robbins JM, Warton K, Bootcov MR, Schofield PR, Campbell TJ, and Breit SN.** Molecular cloning and expression of a chloride ion channel of cell nuclei. *J Biol Chem* 272: 12575–12582, 1997.
26. **Warton K, Tonini R, Fairlie WD, Matthews JM, Valenzuela SM, Qiu MR, Wu WM, Pankhurst S, Bauskin AR, Harrop SJ, Campbell TJ, Curmi PM, Breit SN, and Mazzanti M.** Recombinant CLIC1 (NCC27) assembles in lipid bilayers via a pH-dependent two-state process to form chloride ion channels with identical characteristics to those observed in Chinese hamster ovary cells expressing CLIC1. *J Biol Chem* 277: 26003–26011, 2002.

Peptide Science 2004 : Y. Shimohigashi (Ed.)
The Japanese Peptide Society (2005)

Synthetic Study of an Antigenic Peptide Having a Partial Sequence from *Plasmodium falciparum* Enolase

Kazuto Omi[1], Keisuke Kuriyama[1], Keiichi Yamada[1], Hiroyuki Oku[1], Shigeyuki Kano[2], Kumiko Sato[3], Mamoru Suzuki[4], and Ryoichi Katakai[1]

[1]Department of Chemistry, Gunma University, Gunma 376-8515, Japan, [2]International Medical Center of Japan, Tokyo 162-8655, Japan, [3]Department of Health Sciences, Gunma University, Gunma 371-8511, Japan, and [4]Graduate School of Medicine, Gunma University, Gunma 371-8511, Japan
e-mail: m04c207@gs.eng.gunma-u.ac.jp

The 28-residues peptide having a specific seqeunce from Plasmodium falciparum *enolase* (A^{256}*SEFYNSENKTYDLDFKTPNND*^{277}) *was successfully synthesized by using the combination of stepwise elongation and fragment condensation in solution phase. Fluorescence ELISA data have shown significant reactivity against patients' sera compared with those of healthy volunteers. Thus the peptide has potential applicability as a synthetic antigen such as for diagnnostic usage.*

Keywords: antigen, malaria, peptide, *Plasmodium falciparum* enolase, solution-phase synthesis.

Introduction

Enolase is a key enzyme in the glycolytic pathway and catalyzes the dehydration of 2-phosphoglycerate to 2-phosphopyruvate, which is the ninth reaction in eleven steps pathway from glucose to lactic acid, and the only dehydration reaction in this series [1]. An antigen toward *Plasmodium falciparum* (*P.f.*) enolase has been found in patients' sera [2]. Our previous studies have suggested that a series of partial peptides of *P.f.* enolase have antigenic reactivity against patients' sera. In this study, we have focused on a solution-phase synthesis of an antigenic peptide having a sequence Ala^{256}-Asp^{277} (AD22, Figs 1 and 2) [3], which has been prepared by using solid-phase synthesis in our laboratory. The prepared sequence is shown in Scheme 1.

Results and Discussion

The peptide **1** was synthesized by solution-phase method using both fragment condensation and stepwise coupling procedures as described in Fig. 3. We have chosen *t*-butyloxycarbonyl (Boc) group as α-amino protection. The functional side chains of Asp and Glu were protected with benzyl ester (OBzl). Ser and Thr were protected with benzyl ether (Bzl). Tyr was protected with 2,6-dichlorobenzyl ether(Cl_2-Bzl). Lys was protected with 2-chlorobenzyloxycarbonyl (Cl-Z).

***P.f.* enolase:**	**ASEFYNSENKTYDLDFKTPNND**
Human α-enolase:	ASEFFRSG-K-YDLDFKSPD-D
Human β-enolase:	ASEFYRNG-K-YDLDFKSPD-D
Human γ-enolase:	ASEFYRDG-K-YDLDFKSPT-D

Figure 1. Comparison of amino acid sequences of enolases. A potential antigen, Ala^{256}-Asp^{277} (AD22) in P. f. *enolase and the coresponding segments in Human enolases are shown.*

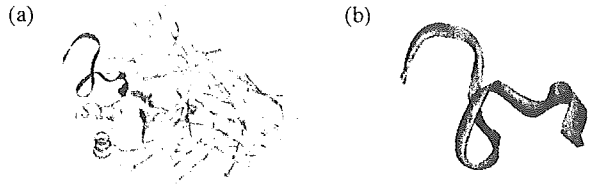

Figure 2. Calculated structure of (a) P.f. *enolase and (b) an antigenic segment (Ala^{256}-Asp^{277}, AD22).*

Scheme 1. The prepared sequence containing 28 amino acid residues (H-Glu_4-AD22-Gly_2-OH, (1)).

Glu-Glu-Glu-Glu-Ala-Ser-Glu-Phe-Tyr-Asn-Ser-Glu-Asn-
Lys-Thr-Tyr-Asp-Leu-Asp-Phe-Lys-Thr-Pro-Asn-Asn-Asp-
Gly-Gly

For the construction of **1**, protected peptide fragments were selected wherein Glu, Leu, Pro and Gly residues were placed at C-terminals, thereby minimizing the danger of racemization during the synthesis. These five fragments were prepared using the stepwise coupling procedure starting from Boc-Xaa-OH (Xaa = Leu, Glu(OBzl) and Pro) or H-Gly-OBzl. Then Boc-Xaa-OH was condensed with trichloroethanol (Tce-OH) to Boc-Xaa-OTce by using dicyclohexylcarbodiimide (DCC) in the presence of 0.1 equimolar of 4-dimethylaminopyridine (DMAP) to supress racemization. Boc group was deprotected by treatment with 4M HCl/dioxane or Trifluoroacetic acid (TFA). Condensation was performed by DCC or 1-ethyl-3-(dimethylaminopropyl)-carbodiimide hydrochloride (EDC.HCl)-hydroxybenzotriazole (HOBt) or 2-(1H-benzotriazole-1-yl)-1,1,3,3-tetramethyluronium hexafluorophosphate (HBTU)-HOBt.

Clude peptides were purified by silicagel, gel filtration chromatography and reprecipitation from appropriate solvents (such as, AcOEt, $CHCl_3$ and THF) by adding hexane. Tce group was deprotected by treatment with Zn/AcOH. Fragment condensation was performed by EDC.HCl-HOBt or O-(7-azabenzo-triazol-1-yl)-1,1,3,3,-tetramethyluronium Hexafluorophospate (HATU). Finally, the protected 28-residues peptide was deprotected by trifluoromethanesulfonic acid (TFMSA)-TFA-thioanisol. The final product was purified by gel-permeation

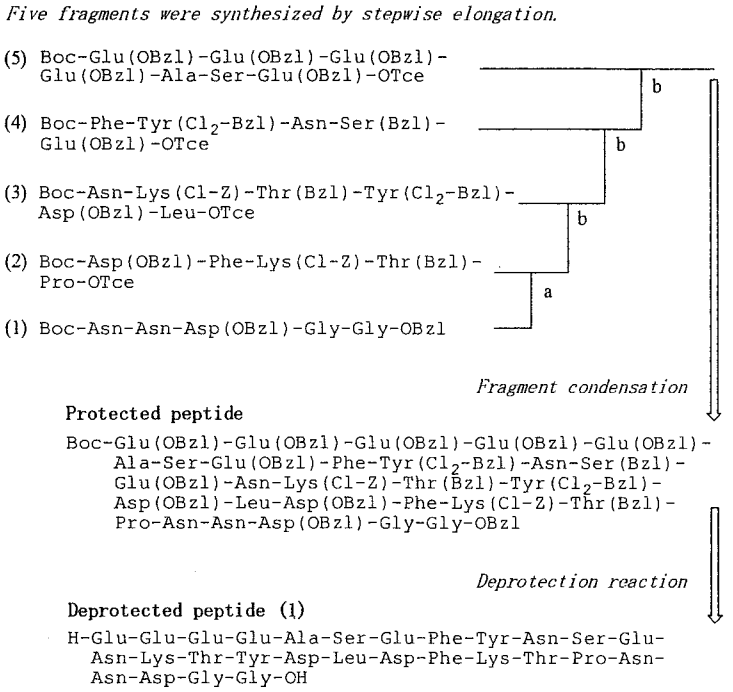

Figure 3. Synthesis of H-Glu$_4$-AD22-Gly$_2$-OH (1). Coupling route of segments are shown. Coupling reagents for segment condensation reactions: a, EDC.HCl-HOBt; b, HATU. All the condensations were performed in DMF. For the final deprotection reaction, the mixture of TFMSA-TFA-thioanisole-m-cresol was used.

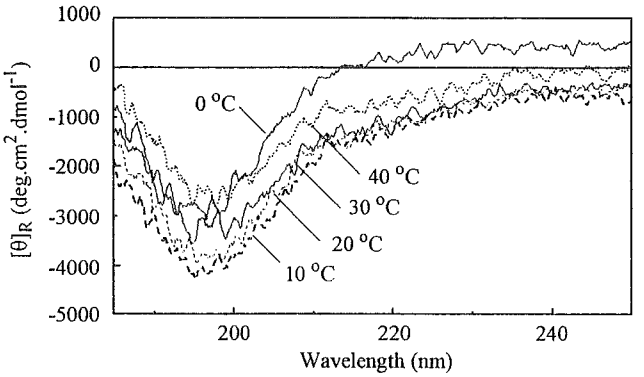

Figure 4. Variable temperature circular dichroism spectra of H-Glu$_4$-AD22-Gly$_2$-OH (1) in phosphate buffer (67 mM, pH 6.4), [1] = 1 mg / ml.

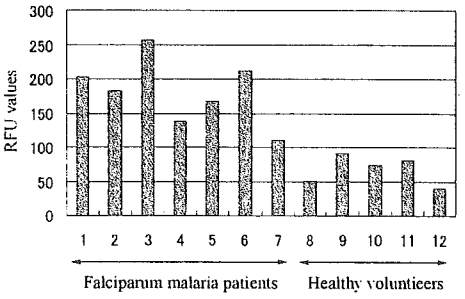

Figure 5. Fluorescence-ELISA Reactivity. The test was performed for the synthetic antigen, H-Glu$_4$-AD22-Gly$_2$-OH (1) (70 μL/well, [1] = 250 μg/mL in 0.05 M carbonate buffer at pH 9.8, reacted at 37°C) against sera from imported falciparum malaria cases in Japan (no. 1-7) and from healthy volunteers (no. 8-12). RFU values (= relative fluorescence unit) are plotted on the ordinate.

chromatography (Sephadex LH60) and HPLC. $[\alpha]_D^{20}$ = -21.3 (c 0.1, DMF); mp, 274-276°C; MALDI-TOF-MS, m/e = 3242.1 ($[M+H]^+$), 3224.1 ($[M+H-H_2O]^+$).

Reactivity of the synthetic peptide, H-Glu$_4$-AD22-Gly$_2$-OH (**1**) against sera from seven cases of imported *falciparum* malaria in Japan and from five healthy volunteers was tested using fluorescence-ELISA (Fig. 5). A considerable degree of the RFU values were measured for patients' sera (mean RFU = 181) compared with those of volunteers (mean RFU = 67).

In conclusion, the ELISA data have suggested that we have successfully synthesized the antigenic peptide suitable for the detection of falciparum malaria. We have expected the potential importance of the antigenic usage and the diagnostic application by further characterization and optimization of the synthetic peptide, **1**.

References

1. (a) Kano, S. (1990) *Japan. J. Trop. Med. Hyg.*, **18**, 317-324. (b) Norazumi, M. K. and Kano, S. (1996) *Japan. J. Trop. Med. Hyg.*, **24**, 223-229.
2. (a) Karasawa, M., Kobayashi, K., Oku, H., Sato, K., Kano, S., Suzuki, M., and Katakai, R. (2000) *Peptide Science 1999*, 295-298. (b) Ishiguro, T., Oku, H., Yamada, K., Sato, K, Kano, S., Suzuki, M., and Katakai, R. (2001) *Peptide Science 2000*, 293-296. (c) R. Nonaka, H. Oku, K., Sato, K, Kano, S., Suzuki, M., and Katakai, R. (2001) *Peptide Science 2000*, 301-304.
3. Jpn. Patent Application, Filing No. 2004-281518.

INFECTION AND IMMUNITY, Nov. 2005, p. 7099–7106 Vol. 73, No. 11
0019-9567/05/$08.00+0 doi:10.1128/IAI.73.11.7099–7106.2005

Shiga Toxin 1 Causes Direct Renal Injury in Rats

Elise T. Yamamoto,[1] Masashi Mizuno,[2] Kiyotaka Nishikawa,[1,3] Shinobu Miyazawa,[1] Lianshan Zhang,[1] Seiichi Matsuo,[2] and Yasuhiro Natori[1]*

Department of Clinical Pharmacology, Research Institute, International Medical Center of Japan, Tokyo 162-8655,[1] Division of Clinical Immunology, Nagoya University Graduate School of Medicine, Nagoya 466-8550,[2] and PRESTO, Japan Science and Technology Agency, Saitama 332-0012,[3], Japan

Received 18 April 2005/Returned for modification 16 June 2005/Accepted 16 August 2005

Infection with Shiga toxin (Stx)-producing *Escherichia coli* has been implicated to cause hemolytic uremic syndrome, which is characterized by histological abnormalities such as microvascular thrombi and tubular cell damage in the kidney. Although Stx is known to be the major virulence factor of the pathogen, it is still unclear whether Stx directly impairs renal cells in vivo to cause such histological changes and deterioration of renal function. To assess the consequence of the direct action of Stx on renal cells, left kidneys of rats were perfused with Stx1 from the renal artery through the renal vein and then revascularized. Kidneys of control animals were perfused with the vehicle alone. On day 1, apoptosis and induction of tumor necrosis factor alpha gene expression were noticed to occur in the medulla of the Stx1-perfused kidneys. On day 3, extensive tubular injuries were observed by light microscopy: aggregated platelets and monocytic infiltrates in both glomeruli and the medullary interstitium were detected by immunostaining. Tubular changes were more extensive on day 9, with areas of infarction seen in the cortex and medulla. These changes were not found to occur in the sham-operated kidneys. No obvious glomerular changes were detected by light microscopy at any time point. When nonperfused right kidneys were removed after the Stx1 perfusion of the left kidneys, the serum creatinine and blood urea nitrogen levels were increased from day 2, and acute renal failure followed on day 3. These results indicate that Stx1 caused glomerular platelet aggregation, tubular damage, and acute deterioration of renal function by acting directly on renal cells.

Hemolytic uremic syndrome (HUS) is a disease defined by nonimmune hemolytic anemia, thrombocytopenia, and acute renal failure (26). Its unique histological features are termed thrombotic microangiopathy, with endothelial cell injury and platelet thrombi being found in the microvasculature (28). HUS, especially in children, is often associated with infection by Shiga toxin (Stx)-producing *Escherichia coli* (STEC), and the clinical and histological abnormalities in these cases are mainly attributed to the action of Stx. Leukocyte infiltration and tubular damage are also noticed as early events in Stx-associated HUS (12, 13).

Stx produced by STEC is classified into two closely related subgroups, Stx1 and Stx2, and both consist of a single enzymatically active A subunit that inactivates 28S rRNA and inhibits protein synthesis and pentameric B subunits that bind to neutral glycolipid globotriaosylceramide (Gb_3), a cell surface receptor. It has been demonstrated that cultured endothelial cells derived from the microvasculature of human tissues such as glomeruli contain high levels of Gb_3 and are highly susceptible to Stx (24). Stx-injured endothelial cells were shown to become adherent to leukocytes (19) and to promote platelet adhesion and thrombus formation (18). Based on these in vitro findings, it has been proposed that Stx directly causes endothelial cell injury in small vessels of the kidney and other target tissues and that the injured endothelial cells then trigger platelet activation and thrombosis in HUS (28). In addition, recent accumulating evidence suggests that renal tubular injury observed with HUS (27) is not only secondary to Stx-induced glomerular and arteriolar injury but also induced by the direct action of Stx on tubular epithelial cells (12). It has been shown that tubular epithelial cells are also highly susceptible to Stx in culture (8). Thus, these studies suggest the existence of a mechanism by which Stx causes HUS via its direct effect on renal cells.

On the other hand, other pathogenic mechanisms operating in HUS in which systemic changes are induced by Stx have also been suggested. It was shown from in vitro studies that Stx binds to (2) and activates (16) platelets, implying that Stx may be directly involved in the prothrombotic state seen with HUS. It was also reported that Stx induced cytokine production in several types of cultured cells (34, 42) and that cytokine levels in the circulation were higher in some patients with Stx-associated HUS (10). In addition, inflammatory cytokines such as tumor necrosis factor alpha (TNF-α) and interleukin-1β were shown to enhance the Gb_3 content and the susceptibility to Stx of cultured endothelial cells (35, 37). Therefore, the effects of Stx on tissues and cells other than those of the kidney may also contribute to the pathological changes observed to occur in the kidneys of patients with HUS.

In contrast to clinical observations on Stx-associated HUS, rodent models induced by systemic administration of Stx or inoculation of STEC show only mild microvascular injury (33). This is probably due to the low level of Gb_3 expression on endothelial cells of the rodent kidney (our unpublished observation). To assess the direct effect of Stx on the kidney, Shibolet et al. (29) perfused isolated rat kidneys with Stx and demonstrated this perfusion to cause marked medullary tubu-

* Corresponding author. Mailing address: Department of Clinical Pharmacology, Research Institute, International Medical Center of Japan, 1-21-1 Toyama, Shinjuku-ku, Tokyo 162-8655, Japan. Phone: 81-3-3202-7181. Fax: 81-3-5273-3038. E-mail: natoriya@ri.imcj.go.jp.

lar injury with no glomerular changes. Their study showed the direct effect of Stx on the kidney, but subsequent events in the Stx-injured kidney could not be analyzed.

The present study was conducted to test the hypothesis that Stx-induced renal damage causes platelet aggregation, tubular injuries, inflammation, and the deterioration of renal function without its systemic action. To this end, we performed Stx1 perfusion of a single kidney, followed by revascularization, in rats. This method allowed us not only to avoid the indirect effects of Stx1 via other tissues or blood but also to analyze interaction, such as platelet activation and leukocyte infiltration, between circulating blood cells and the Stx1-perfused kidney. In addition, because the toxin does not reach the brain in this procedure, we could avoid its fatal attack on the brain (20, 23) and thus administer higher doses of the toxin to cause more-severe damage to the kidney. Also, we could assess the renal function of the perfused kidney by removing the other, nonperfused, healthy kidney. The results of the present study indicate that Stx1 directly caused renal damage that resulted in platelet and monocyte accumulation in glomeruli and medullary interstitium, tubular injuries, and acute deterioration of renal function.

MATERIALS AND METHODS

Materials. Recombinant Stx1 was prepared by using DEAE-Sepharose column chromatography, chromatofocusing column chromatography, and high-performance liquid chromatography, as described previously (21). The 50% cytotoxic dose of the purified Stx1 on Vero cells was around 1 pg/ml. The endotoxin content of the Stx1 preparation was less than 0.016 endotoxin units per 1 mg, as determined by use of an HS-*Limulus* test (Wako Pure Industries, Ltd., Osaka, Japan).

Kidney perfusion. Wistar male rats (240 to 280 g) were obtained from Charles River Japan (Yokohama, Japan) and were allowed free access to chow and water. Handling of rats and experimental procedures were conducted in accordance with institutional guidelines for animal care and use. Kidney perfusion was performed as previously described (17), with slight modifications. Modified Tyrode buffer (17) saturated with 95% oxygen and 5% carbon dioxide and adjusted to pH 7.4 was used as a vehicle. Under anesthesia with pentobarbital, the left kidney of a rat was exposed. Polyethylene tubes were placed in the left renal artery and vein, and the proximal portions of the vessels were temporarily ligated. The left kidney was perfused at a rate of 2 ml/min by using a peristaltic pump. All of the perfusate was discarded through a cannula placed in the renal vein. To eliminate the blood contained inside the kidney, the kidney was perfused first with Tyrode buffer for 30 to 60 s and then with Stx1 (2 μg/ml, in Tyrode buffer containing 1% rat serum) for 3 min. Finally, it was perfused again with the buffer only for 3 min to eliminate any unbound toxin. After the kidney perfusion, the tubes were removed, and the holes in the artery and vein were repaired by microsurgery. Blood circulation of the left kidney was reestablished by releasing the ligature. The average time required for the perfusion procedure was about 15 min. To assess the renal function (see Experiment 2 below), we removed the right kidney just after the perfusion procedure and obtained serum from blood drawn from a tail vein on days 1, 2, and 3 after the revascularization. At sacrifice, pieces of renal tissues were fixed in 10% buffered formalin or snap-frozen in liquid nitrogen. Pieces of renal cortex and medulla were also used for RNA preparation (see below). Levels of serum creatinine and blood urea nitrogen (BUN) were determined colorimetrically by using commercial kits (Wako, Japan).

Morphological studies. Samples fixed in 10% neutral buffered formalin were stained with hematoxylin-eosin and periodic acid-Schiff reagent and used for light-microscopic investigation. To assess tubulointerstitial injuries, kidney sections were arbitrarily divided into four regions, i.e., cortex, outer stripe of the outer medulla, inner stripe of the outer medulla, and inner medulla. In each region, tubulointerstitial changes (dilatation of tubules, degeneration and/or detachment of tubular epithelial cells, and infiltration of inflammatory cells in the interstitial space) were graded from − to +++ as follows: −, normal; +/−, minimal changes; +, changes affecting less than 30% of the area under examination; ++, changes affecting 30 to 60%; and +++, changes affecting more than 60%. For immunohistochemistry, frozen tissues were embedded in OCT compound (Sakura Fine Technical Co., Ltd., Tokyo, Japan), sectioned, washed with phosphate-buffered saline, and incubated with mouse anti-rat monocyte/macrophage monoclonal antibody (ED-1) or anti-rat platelet monoclonal antibody (PL-1, a gift of W. W. Bakker, University Hospital of Groningen, Groningen, The Netherlands). The sections were then incubated with biotinylated horse anti-mouse immunoglobulin G and stained with the reagents of an ABC staining kit (Vector Laboratories, Inc., Burlingame, CA). Monocytes in 30 glomeruli and in 20 consecutive fields of interstitium of a section obtained from each animal were counted in a blind fashion. The total numbers of glomerular and interstitial monocytes/macrophages were expressed as cells per glomerular cross section and cells per mm^2, respectively. Aggregated platelets were semiquantitatively assessed by computer-based measurement of the area of platelet deposition in 30 glomeruli. Apoptotic cells in the kidney were detected by means of the terminal deoxynucleotidyl transferase-mediated dUTP nick end labeling (TUNEL) method using a commercial TACS 2 terminal deoxynucleotidyl transferase kit (Trevigen, Inc., Gaitherburg, MD).

Reverse transcription-PCR. Total RNA fractions were prepared from pieces of renal cortex and medulla by the guanidinium thiocyanate-phenol-chloroform method (1), and 5 μg of RNA was reverse transcribed by use of oligo(dT) primers in 20 μl of buffer as described previously (25). For the quantitative measurement of the TNF-α mRNA levels, real-time PCR was performed by using an ABI PRISM 7700 sequence detector and TaqMan predeveloped assay reagents for gene expression quantification system (Applied Biosystems, Foster City, CA). We assayed the mRNA levels of TNF-α and the endogenous control (GAPDH [glyceraldehyde-3-phosphate dehydrogenase]) by using multiple reporter dyes (Applied Biosystems) and expressed the TNF-α mRNA levels as ratios to the levels of the endogenous control.

Experimental protocol.(i) Experiment 1. A total of 21 rats were perfused with Stx1, and four, four, five, five, and three rats were sacrificed at 1, 6, and 24 h and 3 and 9 days, respectively. As the control, 23 rats were perfused with Tyrode buffer containing 1% rat serum alone and sacrificed at the same time points. The respective numbers of rats sacrificed for the control were four, six, five, four, and four.

(ii) Experiment 2. The left kidneys of four rats were perfused with Stx1 and revascularized as described above, and then their right kidneys were removed. Another group of four control rats was treated in the same way except that they were perfused with the vehicle alone. These animals were sacrificed on day 3.

Statistics. Data were analyzed by the Mann-Whitney U test, and a difference with a P value of <0.05 was considered statistically significant.

RESULTS

Histological changes were first examined by light microscopy. A few changes, such as small areas with detachment of tubular epithelial cells and irregularity of the brush border membranes, were seen for some samples from both sham-operated and Stx1-perfused groups at 6 and 24 h, which possibly resulted from ischemia during the operation; however, no obvious differences between the two groups were found at these time points. On day 3, however, the Stx1-perfused kidneys showed extensive tubular injuries, such as desquamation, cytoplasmic vacuolation, pyknosis, and loss of nuclei. Massive interstitial leukocyte infiltration was also observed to occur in the medulla. On day 9, severe tubular dilatation and degeneration were found to occur in both the cortex and medulla. Typical changes observed by light-microscopic examination are shown in Fig. 1. These abnormalities were not found to occur in the kidneys of sham-operated control rats. No obvious glomerular changes were observed for any animals at any time points. Tubulointerstitial changes in each animal were assessed semiquantitatively (Fig. 2). Statistically significant differences between the two groups were found from day 3 in all areas of the kidney.

Because some changes possibly derived from ischemia were observed to occur in both groups at 6 and 24 h as described above, light-microscopic examination was not appropriate for

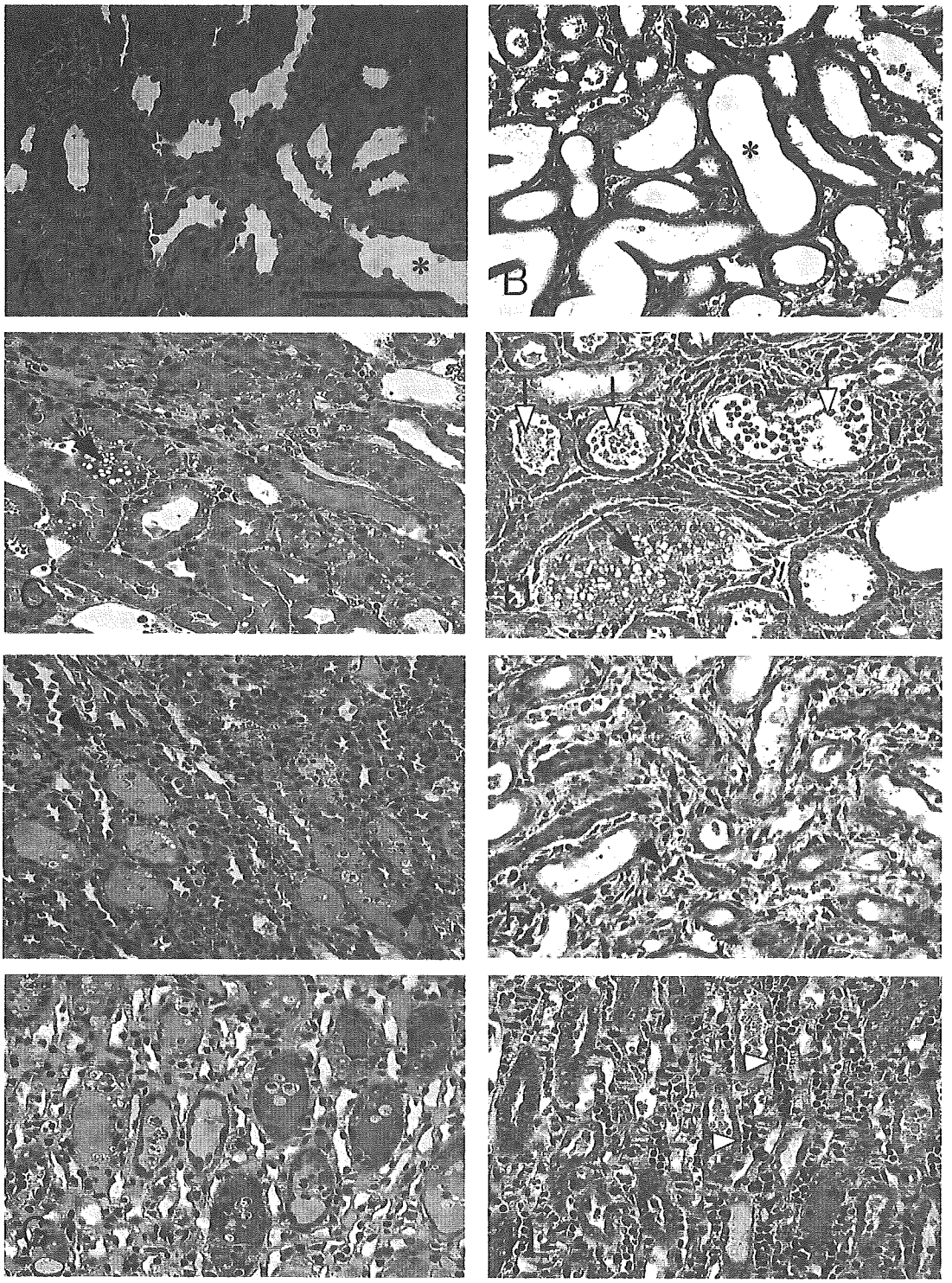

FIG. 1. Typical histological changes in tubulointerstitium of Stx1-perfused and revascularized kidneys seen under light microscopy. Cortex (A and B), outer stripe (C and D), inner stripe (E and F), and inner medulla (G and H) of Stx-perfused kidney on day 3 (A, C, E, and G) and day 9 (B, D, F, and H) postperfusion are shown. Asterisks, tubular dilation; black arrows, cytoplasmic vacuolation; white arrows, desquamation; black arrowheads, leukocyte infiltration; white arrowheads, pyknosis. In the Stx1-perfused kidney, massive infiltration of inflammatory cells is seen on day 3. Severe tubular dilatation and degeneration are notable on day 9. Hematoxylin-eosin staining. Bar, 100 μm.

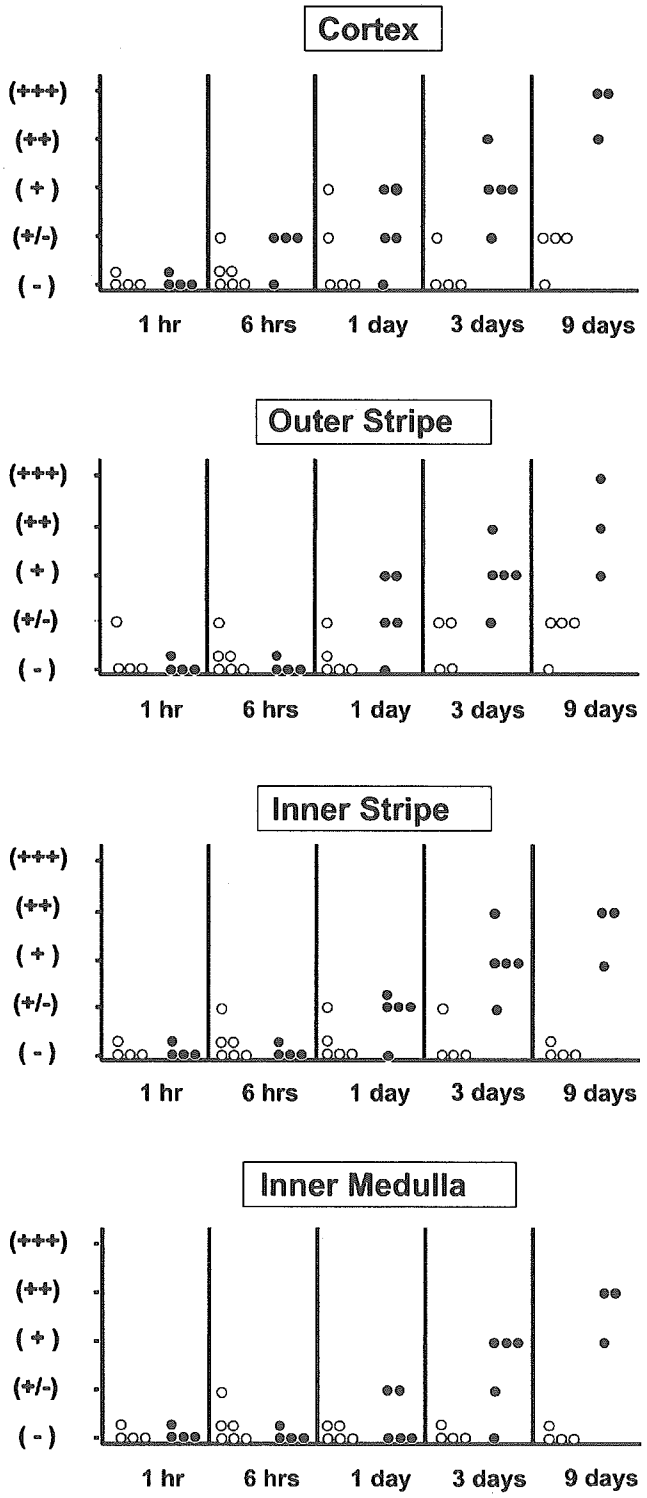

FIG. 2. Semiquantitative analysis of tubulointerstitial injuries seen under light microscopy. Ranking system at left is described in Materials and Methods. Filled circles, Stx-perfused rats; open circles, sham-operated control rats. Each symbol represents one animal. The differences between the two groups on days 3 and 9 in all areas are statistically significant ($P < 0.05$).

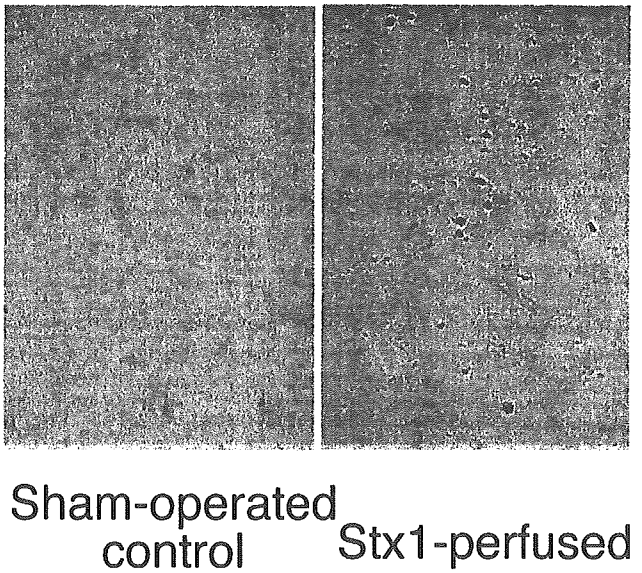

FIG. 3. TUNEL labeling of rat kidneys on day 1. Some tubular cells in the kidneys of Stx-perfused rats were positive for TUNEL staining, but those in the kidneys of the sham-operated rats were not.

analyzing specific effects of Stx1 on renal cells at these time points. Therefore, we examined the kidney sections by TUNEL staining instead. TUNEL-positive cells were detected in the renal medulla of Stx1-perfused animals on day 1 (Fig. 3). Only very few cells in the kidneys of sham-operated animals were positive for TUNEL staining. Almost no TUNEL-positive cells were found in the renal cortex, including glomeruli, for either group.

Activation of renal cells on day 1 was tested by measuring the mRNA levels of TNF-α, an inflammatory cytokine. As

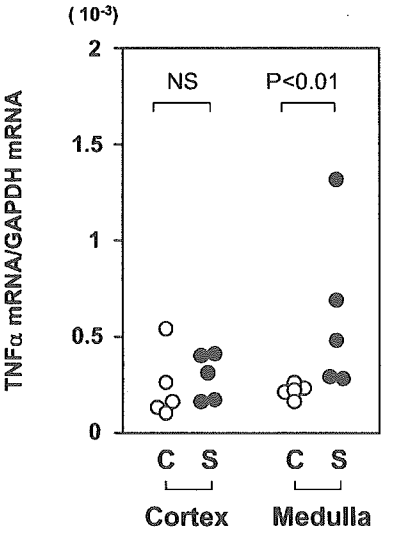

FIG. 4. Expression of TNF-α mRNA in renal cortex and medulla on day 1. Filled circles, Stx-perfused rats (S); open circles, sham-operated control rats (C). Data are expressed as the ratios of the levels of TNF-α mRNA to those of the internal control. Each symbol represents one animal. NS, not significant.

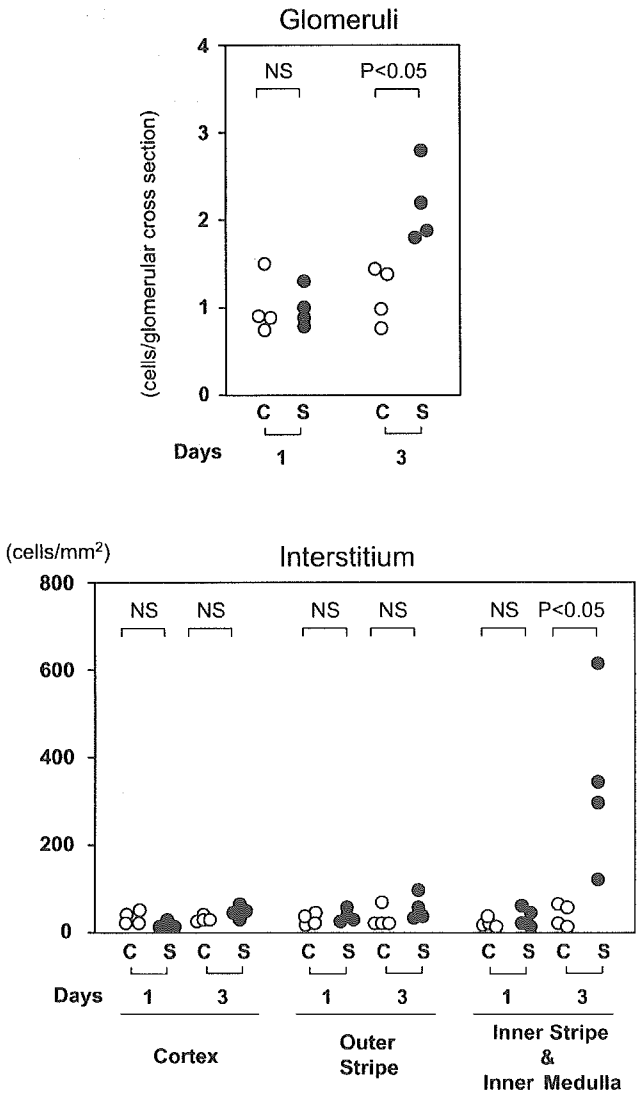

FIG. 5. Monocyte/macrophage infiltration in glomeruli and interstitium on days 1 and 3. Filled circles, Stx-perfused rats (S); open circles, sham-operated control rats (C). Each symbol represents one animal. NS, not significant.

shown in Fig. 4, the levels of TNF-α mRNA in the medulla of Stx1-perfused kidneys were higher than those in the sham-operated kidneys. However, there was no difference in cortical TNF-α mRNA level between the two groups. These results indicate that the perfusion of Stx1 induced apoptosis as well as the gene expression of TNF-α in renal medullary cells.

Next, we tested whether the Stx1 perfusion and revascularization caused accumulation of blood cells in the kidney. On day 1, there was no increase in the number of monocytes/macrophages in the Stx1-perfused kidneys. By day 3, however, evidence of monocyte infiltration was detected in both the glomeruli and the medullary interstitium but not in the cortical interstitium (Fig. 5).

As shown in Fig. 6, platelet aggregation in glomeruli in the Stx1-perfused kidneys but not in the sham-operated kidneys was also detected on day 3 by immunostaining with antiplatelet antibody. The level of platelet aggregation in glomeruli, evaluated by measuring the stained area by computer-analyzed densitometry, confirmed the increase in the glomerular deposition of platelets, suggesting that the injury induced by Stx1 perfusion of the kidney caused platelet aggregation in the glomeruli. Platelet aggregation was also observed to occur in the medullary capillaries.

Finally, to assess the effect of Stx1 on renal function, we removed the right kidneys of the animals just after the Stx1 perfusion. As shown in Fig. 7, levels of serum creatinine and BUN of Stx1-perfused rats were increased from day 2 postperfusion, and acute renal failure followed on day 3. This result clearly shows that Stx1 perfusion and subsequent revascularization caused renal dysfunction.

DISCUSSION

The present study demonstrates that the direct action of Stx1 on the kidney induced (i) apoptosis and TNF-α gene expression in the medulla, (ii) monocyte/macrophage infiltration, (iii) platelet aggregation, (iv) severe tubular damage, and (v) acute deterioration of renal function.

The first abnormalities induced by Stx1 were noticed to occur in the medulla: apoptotic cells, stained by the TUNEL method, and enhanced TNF-α gene expression were detected in the medulla 24 h after Stx1 perfusion. These results are consistent with a previous report (29) that perfusion of Stx in isolated rat kidneys for 160 min caused mainly medullary tubular injuries. Furthermore, apoptotic cells were detected in the kidneys of mice infected with STEC as well as in those of patients with Stx-associated HUS (15, 31). The present study demonstrated that Stx1 by itself induced apoptosis in medullary cells in vivo. Whereas apoptotic cells were detected in the renal cortex in the mouse infection study (15), the present study showed that they were found in the medulla but rarely in the cortex. The difference between these observations may have resulted from the involvement of some virulence factor(s) of the pathogen other than Stx in the mechanism of apoptosis, as suggested earlier (15). The induction of apoptosis by Stx has also been shown for various types of cultured cells, including renal tubular epithelial cells (11, 31).

The induction of TNF by Stx in vivo was also previously reported: an injection of Stx induced TNF biosynthesis in mouse kidney (7) and urinary TNF excretion in baboons (32). With mice, the induction of TNF synthesis by Stx1 was shown only for transgenic animals bearing a chloramphenicol acetyltransferase reporter gene that indicates TNF biosynthesis, as an increase of TNF itself could not be detected (7), suggesting that the cytokine-inducing activity of Stx is relatively weak in rodents. The study also showed that the induction of TNF was kidney specific. In the baboon model, the increase in TNF induced by Stx1 injection was observed with urine but not with serum, and so local TNF production in the kidney was speculated (32). Our results confirmed that speculation and directly showed that Stx1 has the ability to induce expression of the TNF-α gene in vivo, although we did not show it at protein level. In in vitro studies, it has been shown that Stx induced the production of inflammatory cytokines such as TNF-α and interleukin-1 in macrophages (34) and other cultured cells, including tubular epithelial cells (9). Because no increase in the

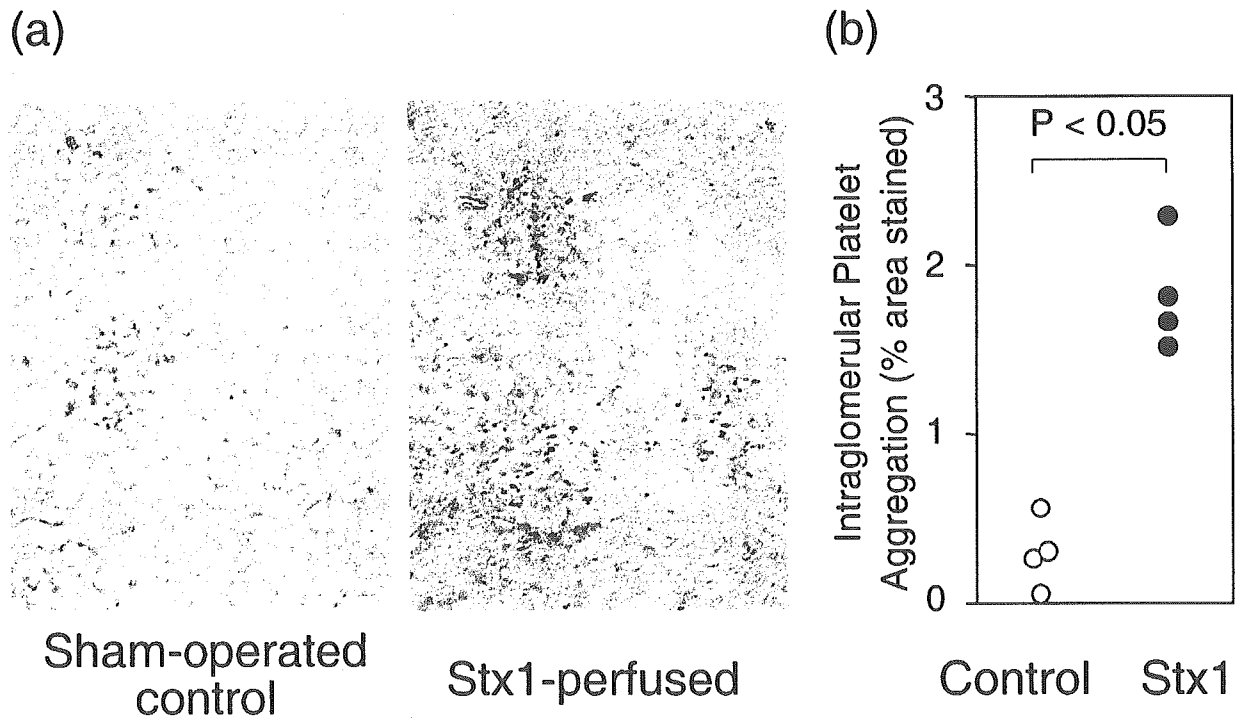

FIG. 6. Glomerular platelet aggregation on day 3. (a) Immunostaining of platelets in glomeruli and (b) quantitative analysis of the platelet aggregation. Glomerular platelet aggregation is expressed as a percentage of the area of glomeruli in cross-section that is occupied by platelets. Filled circles, Stx-perfused rats; open circles, sham-operated control rats. Each symbol represents one animal.

number of medullary macrophages was observed at 24 h after Stx1 perfusion, with the increase in TNF-α mRNA level detected in the medulla, it is conceivable that Stx1 directly induced TNF-α gene expression in intrinsic medullary cells, such as tubular epithelial cells and resident macrophages. In some patients with HUS, an increase in TNF level was observed with both serum and urine (14), but in these cases lipopolysaccharide, a well-known TNF inducer, may also have contributed to TNF production.

Although the induction of both apoptosis and cytokine biosynthesis by Stx has been shown for renal cells (9, 15), it was also reported that both phenomena in the cells can be induced

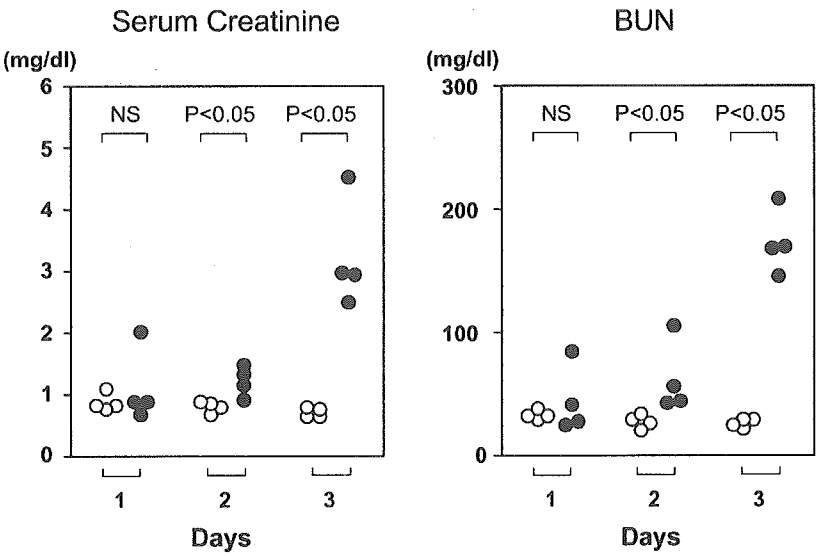

FIG. 7. Levels of serum creatinine and BUN in Stx-perfused rats with uninephrectomy. Filled circles, Stx-perfused rats; open circles, sham-operated control rats. Each symbol represents one animal. NS, not significant.

by ischemia (3, 22) and that tubular cells in the medulla, where these phenomena were observed with the present study, are particularly susceptible to ischemic injury (38). Because our light-microscopic examination showed a few changes in some samples of both sham-operated and Stx1-perfused groups until 24 h, suggesting that these changes potentially resulted from ischemia during the operation, we cannot exclude the possibility that ischemia is involved in the mechanism of the induction of apoptosis and TNF-α. However, the levels of both apoptosis and TNF-α mRNA were significantly higher in Stx1-perfused kidneys than in sham-operated kidneys, and so we consider that Stx1 mainly, if not entirely, contributes to the induction of these activities.

The Stx1 perfusion and subsequent revascularization resulted in monocyte/macrophage infiltration on day 3. This result, together with the finding of TNF induction, suggests that Stx1 itself induces inflammation in the kidney. Although the importance of neutrophils in HUS has been mainly described so far (5), the accumulation of monocytes/macrophages and their role in the pathogenesis of HUS has also been suggested (36). In addition to inducing TNF-α, Stx has been shown to induce chemokine production in some types of cells (34, 42). For example, Simon et al. (30) reported that Stx1 induced monocyte chemoattractant protein 1 production in cultured human mesangial cells. Stx1 also induced the expression of adhesion molecules in endothelial cells (19). In addition to nonspecific, injury-mediated chemoattraction and activation of monocytes, these activities of Stx toward intrinsic renal cells may have contributed to the monocyte infiltration into the kidney.

It has been unclear whether the platelet aggregation observed with HUS is induced directly by Stx or indirectly through Stx-mediated endothelial injury (2, 16, 39, 41). Although no obvious glomerular changes were observed by light microscopy, the present study demonstrates that Stx1 perfusion and revascularization of the rat kidney resulted in platelet aggregation in the glomeruli. This result indicates that the direct action of Stx on platelets is not essential for platelet aggregation and supports the hypothesis that the action of Stx on endothelial cells induces platelet activation in the glomeruli. Because the content of the receptor for Stx, Gb_3, in endothelial cells is much lower in rodents than in humans (our unpublished observation), the level of platelet aggregation was relatively low, and so microthrombotic changes were not observed by light microscopy.

The results of the present study show that Stx directly caused renal damage that began with apoptosis and TNF induction in the medulla, resulting in acute renal failure. The histological changes in the tubulointerstitium were much more prominent than those in the glomeruli. Our result is consistent with previous studies showing that Stx caused much more severe damage to tubules than to glomeruli in rodent kidney (29, 33). Tubular cell damage, in addition to glomerular thrombotic microangiopathy, was observed to occur in patients infected by STEC (27). Although platelet aggregation in glomeruli was observed with the present study, the renal dysfunction may have resulted from the tubular damage rather than from microthrombotic lesions with this model. This may possibly be the case for humans as well.

In contrast to the rodent models, some other animal models have been shown to develop thrombotic microangiopathy, e.g., when baboons were injected with Stx (32) or when greyhound dogs (4), ferrets (40), or gnotobiotic piglets (6) were infected with STEC. As shown in the present study, rats did not develop typical thrombotic microangiopathy, even when perfused with a high dose of Stx. Therefore, this model does not seem to be appropriate for the study of the whole mechanisms of thrombotic microangiopathy, compared with the other models listed above. In addition, indirect effects of Stx through other cells and tissues that may modify the disease are not reflected in the kidney with this model. However, tubulointerstitial injuries, such as apoptosis, inflammation, and resulting renal dysfunction, clearly occurred by the direct action of Stx1 on the kidney, and so we consider that this model provides a new approach for the study of the mechanisms of these events directly caused by Stx in vivo.

ACKNOWLEDGMENTS

We thank W. W. Bakker (University Hospital of Groningen) for providing us the anti-rat platelet antibody and N. Suzuki for his technical advice and assistance.

This work was supported in part by grants from the programs Grants for International Health Cooperation Research (9-S-1) and Health Sciences Research Grants on Emerging and Reemerging Infectious Diseases (H10-ERID-15) of the Ministry of Health, Labor, and Welfare, Japan (to Y.N.).

REFERENCES

1. **Chomczynski, P., and N. Sacchi.** 1987. Single-step method of RNA isolation by acid guanidinium thiocyanate-phenol-chloroform extraction. Anal. Biochem. **162:**156–159.
2. **Cooling, L. L., K. E. Walker, T. Gille, and T. A. Koerner.** 1998. Shiga toxin binds human platelets via globotriaosylceramide (Pk antigen) and a novel platelet glycosphingolipid. Infect. Immun. **66:**4355–4366.
3. **Donnahoo, K. K., X. Meng, A. Ayala, M. P. Cain, A. H. Harken, and D. R. Meldrum.** 1999. Early kidney TNF-α expression mediates neutrophil infiltration and injury after renal ischemia-reperfusion. Am. J. Physiol. **277:** R922–R929.
4. **Fenwick, B. W., and L. A. Cowan.** 1998. Canine model of hemolytic-uremic syndrome, p. 268–277. *In* J. B. Kaper and A. D. O'Brien (ed.), *Escherichia coli* O157:H7 and other Shiga toxin-producing E. *coli* strains. ASM Press, Washington, D.C.
5. **Fitzpatrick, M. M., V. Shah, R. S. Trompeter, M. J. Dillon, and T. M. Barratt.** 1992. Interleukin-8 and polymorphoneutrophil leucocyte activation in hemolytic uremic syndrome of childhood. Kidney Int. **42:**951–956.
6. **Gunzer, F., I. Hennig-Pauka, K. H. Waldmann, R. Sandhoff, H. J. Grone, H. H. Kreipe, A. Matussek, and M. Mengel.** 2002. Gnotobiotic piglets develop thrombotic microangiopathy after oral infection with enterohemorrhagic *Escherichia coli.* Am. J. Clin. Pathol. **118:**364–375.
7. **Harel, Y., M. Silva, B. Giroir, A. Weinberg, T. B. Cleary, and B. Beutler.** 1993. A reporter transgene indicates renal-specific induction of tumor necrosis factor (TNF) by Shiga-like toxin. Possible involvement of TNF in hemolytic uremic syndrome. J. Clin. Investig. **92:**2110–2116.
8. **Hughes, A. K., P. K. Stricklett, and D. E. Kohan.** 1998. Cytotoxic effect of Shiga toxin-1 on human proximal tubule cells. Kidney Int. **54:**426–437.
9. **Hughes, A. K., P. K. Stricklett, and D. E. Kohan.** 1998. Shiga toxin-1 regulation of cytokine production by human proximal tubule cells. Kidney Int. **54:**1093–1106.
10. **Inward, C. D., M. Varagunam, D. Adu, D. V. Milford, and C. M. Taylor.** 1997. Cytokines in haemolytic uraemic syndrome associated with verocytotoxin-producing *Escherichia coli* infection. Arch. Dis. Child **77:**145–147.
11. **Inward, C. D., J. Williams, I. Chant, J. Crocker, D. V. Milford, P. E. Rose, and C. M. Taylor.** 1995. Verocytotoxin-1 induces apoptosis in Vero cells. J. Infect. **30:**213–218.
12. **Kaplan, B. S.** 1998. Shiga toxin-induced tubular injury in hemolytic uremic syndrome. Kidney Int. **54:**648–649.
13. **Kaplan, B. S., K. E. Meyers, and S. L. Schulman.** 1998. The pathogenesis and treatment of hemolytic uremic syndrome. J. Am. Soc. Nephrol. **9:**1126–1133.
14. **Karpman, D., A. Andreasson, H. Thysell, B. S. Kaplan, and C. Svanborg.** 1995. Cytokines in childhood hemolytic uremic syndrome and thrombotic thrombocytopenic purpura. Pediatr. Nephrol. **9:**694–699.
15. **Karpman, D., A. Hakansson, M.-T. R. Perez, C. Isaksson, E. Carlemalm, A.**

Caprioli, and C. Svanborg. 1998. Apoptosis of renal cortical cells in the hemolytic-uremic syndrome: in vivo and in vitro studies. Infect. Immun. **66**:636–644.
16. **Karpman, D., D. Papadopoulou, K. Nilsson, A. C. Sjogren, C. Mikaelsson, and S. Lethagen.** 2001. Platelet activation by Shiga toxin and circulatory factors as a pathogenetic mechanism in the hemolytic uremic syndrome. Blood **97**:3100–3108.
17. **Matsuo, S., F. Yoshida, Y. Yuzawa, S. Hara, A. Fukatsu, Y. Watanabe, and N. Sakamoto.** 1989. Experimental glomerulonephritis induced in rats by a lectin and its antibodies. Kidney Int. **36**:1011–1121.
18. **Morigi, M., M. Galbusera, E. Binda, B. Imberti, S. Gastoldi, A. Remuzzi, C. Zoja, and G. Remuzzi.** 2001. Verotoxin-1-induced up-regulation of adhesive molecules renders microvascular endothelial cells thrombogenic at high shear stress. Blood **98**:1828–1835.
19. **Morigi, M., G. Micheletti, M. Figliuzzi, B. Imberti, M. A. Karmali, A. Remuzzi, G. Remuzzi, and C. Zoja.** 1995. Verotoxin-1 promotes leukocyte adhesion to cultured endothelial cells under physiologic flow conditions. Blood **86**:4553–4558.
20. **Nishikawa, K., K. Matsuoka, E. Kita, N. Okabe, M. Mizuguchi, K. Hino, S. Miyazawa, C. Yamasaki, J. Aoki, S. Takashima, Y. Yamakawa, M. Nishijima, D. Terunuma, H. Kuzuhara, and Y. Natori.** 2002. A therapeutic agent with oriented carbohydrates for treatment of infections by Shiga toxin-producing *Escherichia coli* O157:H7. Proc. Natl. Acad. Sci. USA **99**:7669–7674.
21. **Noda, M., T. Yutsudo, N. Nakabayashi, T. Hirayama, and Y. Takeda.** 1987. Purification and some properties of Shiga-like toxin from *Escherichia coli* O157:H7 that is immunologically identical to Shiga toxin. Microb. Pathog. **2**:339–349.
22. **Nogae, S., M. Miyazaki, N. Kobayashi, T. Saito, K. Abe, H. Saito, P. K. Nakane, Y. Nakanishi, and T. Koji.** 1998. Induction of apoptosis in ischemia-reperfusion model of mouse kidney: possible involvement of Fas. J. Am. Soc. Nephrol. **9**:620–631.
23. **O'Brien, A. O., T. A. Lively, M. E. Chen, S. W. Rothman, and S. B. Formal.** 1983. *Escherichia coli* O157:H7 strains associated with haemorrhagic colitis in the United States produce a *Shigella dysenteriae* 1 (Shiga) like cytotoxin. Lancet **i**:702.
24. **Obrig, T. G.** 1998. Interaction of Shiga toxins with endothelial cells, p. 303–311. *In* J. B. Kaper and A. D. O'Brien (ed.), *Escherichia coli* O157:H7 and other Shiga toxin-producing E. *coli* strains. ASM Press, Washington, D.C.
25. **Ou, Z. L., Y. Natori, N. Doi, K. Kawasaki, M. Nishijima, and Y. Natori.** 1998. Competitive reverse transcription-polymerase chain reaction for determination of rat CC and C chemokine mRNA and its application to experimental glomerulopathy. Anal. Biochem. **261**:227–229.
26. **Remuzzi, G., and P. Ruggenenti.** 1995. The hemolytic uremic syndrome. Kidney Int. **48**:2–19.
27. **Richardson, S. E., M. A. Karmali, L. E. Becker, and C. R. Smith.** 1988. The histopathology of the hemolytic uremic syndrome associated with verocytotoxin-producing *Escherichia coli* infections. Hum. Pathol. **19**:1102–1108.
28. **Ruggenenti, P., M. Noris, and G. Remuzzi.** 2001. Thrombotic microangiopathy, hemolytic uremic syndrome, and thrombotic thrombocytopenic purpura. Kidney Int. **60**:831–846.
29. **Shibolet, O., A. Shina, S. Rosen, T. G. Cleary, M. Brezis, and S. Ashkenazi.** 1997. Shiga toxin induces medullary tubular injury in isolated perfused rat kidneys. FEMS Immunol. Med. Microbiol. **18**:55–60.
30. **Simon, M., T. G. Cleary, J. D. Hernandez, and H. E. Abboud.** 1998. Shiga toxin 1 elicits diverse biologic responses in mesangial cells. Kidney Int. **54**:1117–1127.
31. **Taguchi, T., H. Uchida, N. Kiyokawa, T. Mori, N. Sato, H. Horie, T. Takeda, and J. Fujimoto.** 1998. Verotoxins induce apoptosis in human renal tubular epithelium derived cells. Kidney Int. **53**:1681–1688.
32. **Taylor, F. J., V. L. Tesh, L. DeBault, A. Li, A. C. Chang, S. D. Kosanke, T. J. Pysher, and R. L. Siegler.** 1999. Characterization of the baboon responses to Shiga-like toxin: descriptive study of a new primate model of toxic responses to Stx-1. Am. J. Pathol. **154**:1285–1299.
33. **Tesh, V. L., J. A. Burris, J. W. Owens, V. M. Gordon, E. A. Wadolkowski, A. D. O'Brien, and J. E. Samuel.** 1993. Comparison of the relative toxicities of Shiga-like toxins type I and type II for mice. Infect. Immun. **61**:3392–3402.
34. **Tesh, V. L., B. Ramegowda, and J. E. Samuel.** 1994. Purified Shiga-like toxins induce expression of proinflammatory cytokines from murine peritoneal macrophages. Infect. Immun. **62**:5085–5094.
35. **van de Kar, N. C. A. J., L. A. H. Monnens, M. A. Karmali, and V. W. M. van Hinsbergh.** 1992. Tumor necrosis factor and interleukin-1 induce expression of the verocytotoxin receptor globotriaosylceramide on human endothelial cells: implications for the pathogenesis of the hemolytic uremic syndrome. Blood **80**:2755–2764.
36. **van Setten, P. A., V. W. M. van Hinsbergh, L. P. W. J. van den Heuvel, F. Preyers, H. B. P. M. Dijkman, K. J. M. Assmann, T. J. A. M. van der Velden, and L. A. Monnens.** 1998. Monocyte chemoattractant protein-1 and interleukin-8 levels in urine and serum of patents with hemolytic uremic syndrome. Pediatr. Res. **43**:759–767.
37. **van Setten, P. A., V. W. M. van Hinsbergh, T. J. A. N. van der Velden, N. C. A. J. van de Kar, M. Vermeer, J. D. Mahan, K. J. M. Assmann, L. P. W. J. van den Heuvel, and L. A. H. Monnens.** 1997. Effects of TNFα on verocytotoxin cytotoxicity in purified human glomerular microvascular endothelial cells. Kidney Int. **51**:1245–1256.
38. **Vetterlein, F., A. Petho, and G. Schmidt.** 1986. Distribution of capillary blood flow in rat kidney during postischemic renal failure. Am. J. Physiol. **251**: H510–H519.
39. **Viisoreanu, D., R. Polanowska-Grabowska, S. Suttitanamongkol, T. G. Obrig, and A. R. Gear.** 2000. Human platelet aggregation is not altered by Shiga toxins 1 or 2. Thromb. Res. **98**:403–410.
40. **Woods, J. B., C. K. Schmitt, S. C. Darnell, K. C. Meysick, and A. D. O'Brien.** 2002. Ferrets as a model system for renal disease secondary to intestinal infection with *Escherichia coli* O157:H7 and other Shiga toxin-producing *E. coli*. J. Infect. Dis. **185**:550–554.
41. **Yagi, H., N. Narita, M. Matsumoto, Y. Sakurai, H. Ikari, A. Yoshioka, E. Kita, Y. Ikeda, K. Titani, and Y. Fujimura.** 2001. Enhanced low shear stress induced platelet aggregation by Shiga-like toxin 1 purified from *Escherichia coli* O157. Am. J. Hematol. **66**:105–115.
42. **Yamasaki, C., Y. Natori, X.-T. Zeng, M. Omura, S. Yamasaki, Y. Takeda, and Y. Natori.** 1999. Induction of cytokines in a human colon epithelial cell line by Shiga toxin-1 (Stx1) and Stx2 but not by nontoxic mutant Stx1 which lacks *N*-glycosidase activity. FEBS Lett. **442**:231–234.

Editor: D. L. Burns

GASTROENTEROLOGY 2005;128:411–423

Therapeutic Potential of Follistatin for Colonic Inflammation in Mice

TAEKO DOHI,* CHIEKO EJIMA,* RIE KATO,* YUKI I. KAWAMURA,* REI KAWASHIMA,* NORIKO MIZUTANI,* YOSHIAKI TABUCHI,† and ITARU KOJIMA§

*Department of Gastroenterology, Research Institute, International Medical Center of Japan, Tokyo; †Division of Molecular Genetics, Life Scientific Research Center, Toyama Medical and Pharmaceutical University, Toyama; and §Institute for Molecular and Cellular Regulation, Gunma University, Maebashi, Japan

Background & Aims: Activins belong to the transforming growth factor-β superfamily. Recent studies have shown that activin and its natural antagonist, follistatin, are involved in tissue repair and inflammatory processes. The aim of this study was to determine whether neutralization of activins with follistatin would have an in vivo anti-inflammatory effect in several murine models of colitis. *Methods:* We assessed activin levels in the colitis induced by intracolonic administration of trinitrobenzene sulfonic acid (TNBS). We subsequently tested the effects of an intraperitoneal injection of follistatin before or after induction of TNBS colitis. We also examined the established colitis induced by oral dextran sulfate sodium (DSS) as well as the spontaneous colitis that develops in interleukin (IL)-10 gene-deficient (IL-10$^{-/-}$) mice. *Results:* Levels of activin transcripts in the colon during the acute phase of TNBS colitis were up-regulated. Epithelial cells, infiltrating macrophages (Mϕ), and endothelial cells produced excess activin βA. Pretreatment with follistatin increased the survival rate of mice with TNBS colitis from 33% to 82% and decreased the plasma levels of IL-6 and amyloid A. Administration of follistatin also reduced the histologic score and tissue myeloperoxidase activity in established TNBS and DSS colitis and reduced the severity of the colitis in IL-10$^{-/-}$ mice. Based on results obtained from 3 mouse models and from in vitro experiments, follistatin promoted the proliferation of colonic epithelial cells. *Conclusions:* Neutralization of activins by follistatin promoted epithelial cell division and tissue repair, clearly suggesting a treatment modality for intestinal inflammation.

The maintenance of the architectural features of the gastrointestinal (GI) tract is not a static process but instead occurs through vigorous and rapid cell regeneration. Epithelial cells arise by a process of clonal growth from stem cells present in the deep crypts, and progeny cells move in vertical columns toward the villus apex. In the small intestine, cells produced by mitosis in the crypt live only 2–3 days before reaching the villus tip and are then extruded.[1] These progeny cells, which differentiate into either absorptive or goblet cells, form a potent tissue polarity. This continuous renewal of the intestinal epithelium is also important for the regeneration of tissues damaged by inflammation. In addition to growth factors, both inflammatory cytokines and chemokines also contribute to this normal tissue repair.

Activins belong to the transforming growth factor-β (TGF-β) superfamily and have numerous biologic effects on the proliferation and differentiation of several types of cells. Different forms of activin are known: (1) Activin A is a homodimer of activin βA subunits; (2) activin B is a homodimer of activin βB subunits; and (3) activin AB is a heterodimer of these 2 subunits.[2] Activin βC, βD, and βE subunits also occur in mammals. The actions of the activins are controlled by the synthesis and expression of type I and type II receptors, as well as by the natural antagonist follistatin, which binds activins A and B with high affinity and blocks their function.[3,4] Another activin-binding protein, follistatin-like protein 3, was recently discovered, and its differential binding and neutralization of activins were described.[5] In general, activin A is considered to be an autocrine factor for regulating the growth and differentiation of epithelial cells, including renal tubular cells[6] and hepatocytes.[7] There are several studies that have addressed the expression of activins in the GI tract, in which significant cell proliferation occurs. Activin synthesis was detected in a human embryonic intestinal cell line,[8] in the human colonic cancer cell line Caco 2, and in the rat intestine.[9] Exogenous activin A suppressed the proliferation of IEC-6 cells in a dose-dependent manner.[10] Recent studies have clearly

Abbreviations used in this paper: BrdU, bromodeoxyuridine; DIG, digoxygenin; DSS, sodium dextran sulfate; IL, interleukin; IL-10$^{-/-}$, IL-10 gene deficient; LPMCs, lamina propria mononuclear cells; Mϕ, macrophages; TGF-β, transforming growth factor-β; TNBS, trinitrobenzene sulfonic acid; TNP, trinitrophenyl.

0016-5085/05/$30.00
doi:10.1053/j.gastro.2004.11.063

shown an important role for activins in systemic inflammatory responses and tissue repair.[11–13] A potential role for activins in inflammatory bowel disease (IBD) was suggested by the following findings: No activin βA messenger RNA (mRNA) was present in the normal human GI tract; however, the levels of mRNA for activin βA positively correlated with the degree of inflammation in IBD patients, as manifested by histopathology and by an increase in the level of interleukin (IL)-1β.[14] Activin receptors I and II were present throughout the GI tract of patients with IBD and in control subjects. In contrast, no expression of the activin βA protein was noted in controls, whereas βA was expressed in the intestinal tissues of the patients.[10]

In the present study, we investigated the expression of activins and follistatin in the inflamed murine intestinal tract in a colitis model prepared by colonic administration of trinitrobenzene sulfonic acid (TNBS). We were successful in treating colitis by neutralizing the action of activin through administration of follistatin in both the TNBS and oral dextran sulfate sodium (DSS) colitis models, as well as in IL-10 gene-deficient (IL-$10^{-/-}$) mice, which develop colitis spontaneously.

Materials and Methods

Mice

Female 8-week-old BALB/c mice obtained from CLEA Japan Inc. (Tokyo, Japan) were maintained under pathogen-free conditions in a facility of the Research Institute, International Medical Center of Japan (IMCJ; Tokyo, Japan). IL-$10^{-/-}$ mice (C57BL/6 background)[15] were purchased from the Jackson Laboratory (Bar Harbor, ME). All experiments were performed according to the Institutional Guidelines for the Care and Use of Laboratory Animals in Research and the approval of the local ethics committee in the IMCJ.

Induction of Colitis and Administration of Follistatin

TNBS colitis was induced as described previously.[16,17] A 2% solution of TNBS (Research Organics, Cleveland, OH) in PBS:ethanol (1:1 by volume) was administered intrarectally to mice lightly anesthetized with ketamine (Sankyo Co. Ltd., Tokyo, Japan). Different doses of TNBS were used according to the requirements of each experiment. For comparison of the survival rate and analysis of acute inflammatory parameters at day 1, a dose of 60 μg/g (3 μL solution/g) body weight of TNBS was given, which caused death in approximately 20% and 70% of BALB/c mice within 24 hours and 72 hours, respectively, following the TNBS enema. For histologic and time-course analyses, a TNBS dose of 48 μg/g of body weight was administered, and this resulted in the death of 10% or 40% of the mice at 24 hours and 72 hours, respectively (data not shown). Specimens for analysis were collected among the surviving mice at each time point after death with an excess intraperitoneal (i.p.) injection of a mixture of ketamine and xylazine. Human recombinant follistatin was kindly provided by Dr. Yuzuru Eto (Ajinomoto Co., Inc., Tokyo, Japan). An aliquot of follistatin (5 μg in 0.1 mL in PBS with 0.5% normal mouse serum) was injected i.p. 30 minutes prior to the TNBS administration. Control groups received an injection of PBS containing 0.5% normal mouse serum. To examine the effects of follistatin on established TNBS colitis, we administered a TNBS dose of 48 μg/g of body weight on day 0 and day 7, as described previously[16] and then 5 μg follistatin on day 8.

For induction of dextran sulfate sodium (DSS)-colitis, DSS (M. W. 5000; Sigma-Aldrich Co., Inc, Tokyo, Japan) was added to the drinking water at the concentration of 2%. Mice were provided this water ad libitum. After 7 days, weight loss was not yet obvious; however, most of the mice exhibited bloody diarrhea, and histologic analysis revealed colitis. Follistatin (5 μg) was then given IP to DSS-treated mice on days 7, 9, and 11. The drinking water was supplemented with DSS continuously until day 12 for all groups of mice. On day 12, the colon was resected for analysis. To test the effects of follistatin on the recovery phase of DSS colitis, we gave mice a 5% solution of DSS for 8 days and then administered 5 μg follistatin on days 7, 9, and 11. Histologic examination was done at day 14 in this group.

IL-$10^{-/-}$ mice, maintained in the IMCJ specific pathogen-free facility, were free from signs of enteritis, and a set of female littermates born within a week of each other from 2 breeder female mice were placed in a conventional environment, in which no major pathogens were detected, at the age of 7 weeks. Four weeks after transferring these mice to this environment, all mice showed transient anal prolapse upon defecation with soft feces; however, their general condition was not affected, and no weight loss was seen. At the age of 18 weeks, their condition remained stable, and administration of follistatin was initiated. These littermates were separated into 2 groups based on their body weight, and 1 group was given follistatin (5 μg) IP on days 0, 3, 6, and 9. The other control group received an injection of PBS containing 0.5% normal mouse serum. On day 12, colonic tissue samples were taken for histologic analysis. This experiment was also performed on a separated set of male littermates, which were kept in the conventional environment for only 4 weeks.

In Situ Hybridization

Digoxygenin (DIG)-labeled activin βA antisense and sense probes were prepared by in vector transcription by using a DIG RNA labeling Kit (Roche Diagnostics GmbH, Mannheim, Germany). In brief, a 1.6-kb *Xho*I fragment from the human activin βA coding sequence was cloned into pSPT18 and pSPT19. Sense cRNA was transcribed from pSPT18 with SP6 polymerase, and antisense cRNA was transcribed from pSPT19 with T7 polymerase. Mouse tissues were snap-frozen and embedded in O.C.T. compound (Sakura Finetechnical Co. Ltd. Tokyo. Japan). Eight-μm-thick sections were prepared, dried briefly, and fixed with 4% paraformaldehyde in PBS for

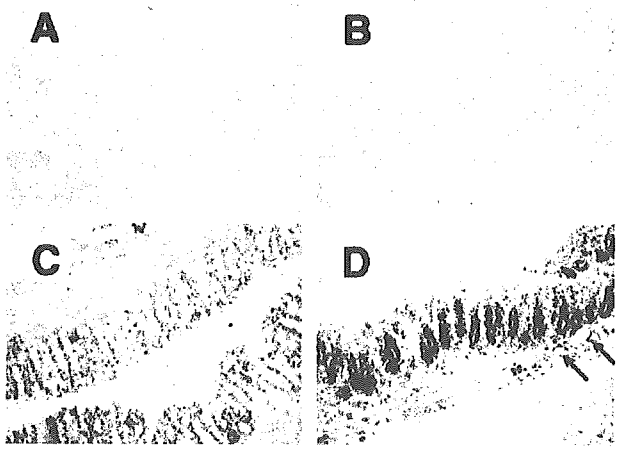

Figure 1. Up-regulation of activin βA mRNA was determined by in situ hybridization. Colonic tissues obtained 24 hours after intracolonic TNBS administration (48 μg/g; *B* and *D*) and those from naïve mice (*A* and *C*) were incubated with either sense (*A* and *B*) or antisense (*C* and *D*) probes for activin βA. Pictures chosen are representative of specimens from 4 mice for each group. The *arrows* indicate endothelial cells.

10 minutes. After digestion with 0.8 mg/mL Proteinase K (DakoCytomation Inc., Kyoto Japan) for 6 minutes and fixation with 4% PFA at 4°C for 20 minutes, the sections were treated with acetic anhydride and then incubated at 50°C overnight in hybridization buffer containing 1 μg/mL DIG-labeled cRNA, as described previously.[18] After hybridization, the sections were washed and incubated with RNAse A (Sigma Chemical Co., St. Louis, MO). The hybridized probe was detected with a DIG Nucleic Acid Detection Kit (Roche Diagnostics, Indianapolis, IN), used according to the manufacturer's protocol.

Cell Separation and Culture

Samples of large intestine were taken, opened longitudinally, and rinsed in PBS. They were then treated with 2 mmol/L EDTA in PBS for 30 minutes to remove the epithelial cells. The residue was completely denuded from epithelial cells by vigorous washing and then digested with type V collagenase (Sigma) for 20 minutes to obtain lamina propria mononuclear cells (LPMCs). This step was repeated once more. In some experiments, the LPMCs were resuspended in RPMI 1640 supplemented with 5% FCS, penicillin, streptomycin, and amphotericin B (RPMI 1640 medium) in 48-well plates (3×10^6 cells/well) and incubated in a humidified 5% CO_2 incubator for 45 minutes. The nonadherent cells, removed by washing with RPMI 1640 medium 3 times, and the remaining adherent cells were both used in further experiments. In some experiments, nonadherent cells were further purified with biotinylated anti-CD3 or anti-B 220 mAbs (BD Pharmingen, San Diego, CA) and a magnetic cell separator (AutoMACS, Miltenyi Biotec GmbH, Germany). To assess activin A release in cultures, we incubated cells in RPMI 1640 supplemented with 10% FCS, sodium pyruvate, L-glutamine, HEPES, penicillin, streptomycin, and amphotericin B (complete medium) at 37°C in an atmosphere of 5% CO_2 in air. After 24 hours of culture, the supernatants were removed and subjected to an ELISA, as described below. Cells of the murine colonic epithelial cell line MCE301[19] were cultured in collagen-coated dishes or in BD Biocoat Cell Culture Inserts coated with collagen I (Becton Dickinson Co., Franklin Lakes, NJ) in DME/F12 medium supplemented with ITES, 10 ng/mL EGF, and 2% FCS at 33°C. After the cells had reached confluence, they were cultured at the nonpermissive temperature (39°C) for 3 days to induce differentiation and used for experiments. The human colonic cell line HT-29 (American Type Culture Collection, Rockville, MD) was cultured in Dulbecco's modified Eagle medium containing 10% fetal bovine serum. In some experiments, recombinant human activin A (Techne Co., Minneapolis, MN) or follistatin was added to the cultures. For the TNBS-specific T-cell proliferation assay, mononuclear cells were isolated from sacral lymph nodes and treated with 0.3 mg/mL TNBS in RPMI 1640 for 15 minutes at room temperature. They were then extensively washed and cultured in complete medium for 3 days. In each well of 96-well plates, 2×10^5 cells were placed, and 0.5 μCi/well of tritiated [^{3}H] thymidine was added 18 hours before harvesting of the cells. The amount of [^{3}H] thymidine was determined by scintillation counting. The proliferation index was determined as counts per minute (cpm) of wells with TNBS/cpm of wells without TNBS.

Histologic Analysis

The GI tract tissues were taken, fixed in 5% glacial acetic acid in ethanol, and paraffin-embedded; then 4-μm sections were prepared and stained with H&E. The colon was cut into upper, middle, and lower parts for histopathologic analysis. In some experiments, frozen sections were also used. To visualize proliferating cells, we injected 1 mg bromodeoxyuridine (BrdU, Sigma) i.p. 1 hour before death. Paraffin-embedded sections were treated with 4 N HCl, blocked with 1% bovine serum albumin in PBS, and stained with rat anti-BrdU Ab (Oxford Biotech, Ltd, Oxford, United Kingdom), followed by FITC-labeled anti-rat IgG Ab (Southern Biotechnology Associates, Inc. [SBA], Birmingham, AL). The numbers of $BrdU^+$ cells per crypt were counted, and at least 20 crypts in 3 separate fields were examined in each section. Histologic scores for TNBS colitis were determined as previously described.[17] Histologic scores for DSS colitis were determined by summing scores for changes in the epithelium (0, normal; 1, focal loss of goblet cells; 2, diffuse loss of goblet cells; 3, focal loss of crypts; 4, diffuse loss of crypts) and for cell infiltration (0, no increase; 1, around bases of the crypts; 2, diffuse infiltration along the layer of Muscularis mucosae; 3, complete infiltration of the mucosal layer; 4, infiltration of both mucosal and submucosal layers). Scores for stool consistency and rectal bleeding were assessed according to previously published procedures.[20] For detection of activin receptor IIB, a rabbit polyclonal antibody was kindly provided by Dr. Kohei Miyazono (The University of Tokyo). Frozen sections fixed with cold acetone for 10 minutes

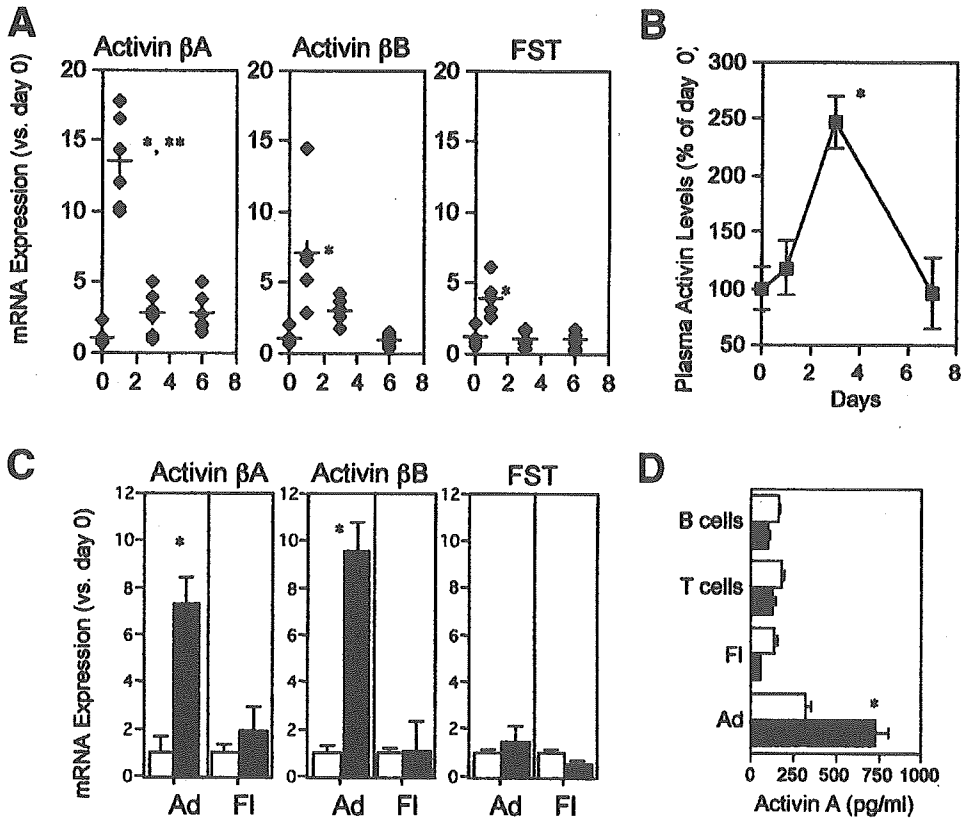

Figure 2. Activin expression was up-regulated during the acute phase of TNBS colitis. (*A*) Mice were given TNBS (48 μg/g) on day 0. Total RNA was extracted from the colon on the days indicated, and mRNA for activin βA, activin βB, and follistatin were analyzed by quantitative RT-PCR. The results from 6 mice/datum point are shown, and the results indicated as (+) are the average of each group. *Statistically significant difference from other time points in each graph. **Statistically significant difference from activin βB and follistatin at day 1 ($P < .05$). (*B*) Plasma levels of activin A after induction of TNBS colitis. Results are expressed as a percentage of the level at day 0 (naïve mice) and are shown as the average of 5 mice/group and the standard deviation. (*C*) Increased levels of activin transcripts in colonic adherent cells in the acute phase of TNBS colitis. Six hours after intracolonic administration of TNBS, adherent (*Ad*) and floating (*Fl*) cells were obtained from pooled colonic LPMC of 3 mice, and the total RNA was extracted for quantitative RT-PCR analysis (*solid column*), which was done in triplicate. Results are shown as expression relative to that in the same cell fraction obtained from naïve mice not given TNBS (*open column*). Three independent pools of RNA from different mouse groups gave similar results. *Differences from naïve mice were statistically significant ($P < .05$). (*D*) Increased release of activin A by colonic adherent LPMC in TNBS colitis. Six hours after intracolonic administration of TNBS, adherent (*Ad*) and total floating (*Fl*) cells were obtained from LPMCs pooled from 3 mice and cultured for 24 hours (0.5×10^6 cells/mL). The culture supernatants were then assessed for activin A by ELISA. $CD3^+$ (*T cells*) and $B220^+$ (*B cells*) cells separated by magnetic sorting from the floating cell fraction were also tested. Representative data from 3 experiments are shown.

were treated with Blockace (Dainippon Pharmaceuticals, Osaka, Japan), incubated with the antiactivin receptor IIB antibody (1:100 dilution) for 60 minutes then reacted with TRITC-labeled anti-rabbit IgG secondary antibody (SBA).

ELISA

Activin A in culture supernatants and in plasma was measured by using a Quantikine M mouse activin A immunoassay kit (R&D Systems, Minneapolis, MN). Both IL-6 and tumor necrosis factor (TNF)-α were assessed with an ELISA development kit (Techne Co., Minneapolis, MN). Plasma levels of amyloid A were quantified by using a Cytoscreen immunoassay kit (BioSource International, Inc. Camarillo, CA). Murine MCP-1 and human IL-8 in culture medium were determined with an ELISA Kit purchased from Pierce Endogen (Rockford, IL).

Myeloperoxidase Assay

The myeloperoxidase (MPO) activity in colonic tissues was determined by a method reported previously.[21] Briefly, colonic tissues were homogenized in 5 mmol/L phosphate buffer (pH 6.0) and centrifuged at 30,000*g* for 30 minutes at 4°C. The pellet was suspended in 50 mmol/L phosphate buffer containing 0.5% hexadecyltrimethyl ammonium bromide. After centrifugation at 20,000*g*, the supernatant was subjected to the MPO assay by use of a spectrophotometer equipped with a rate assay system (U3200; Hitachi, Tokyo, Japan). Data were presented as MPO activity units/g tissue.

RT-PCR for mRNA Analysis

Total RNA was prepared from colonic tissue or from separated cells by using RNA-Bee RNA isolation reagent

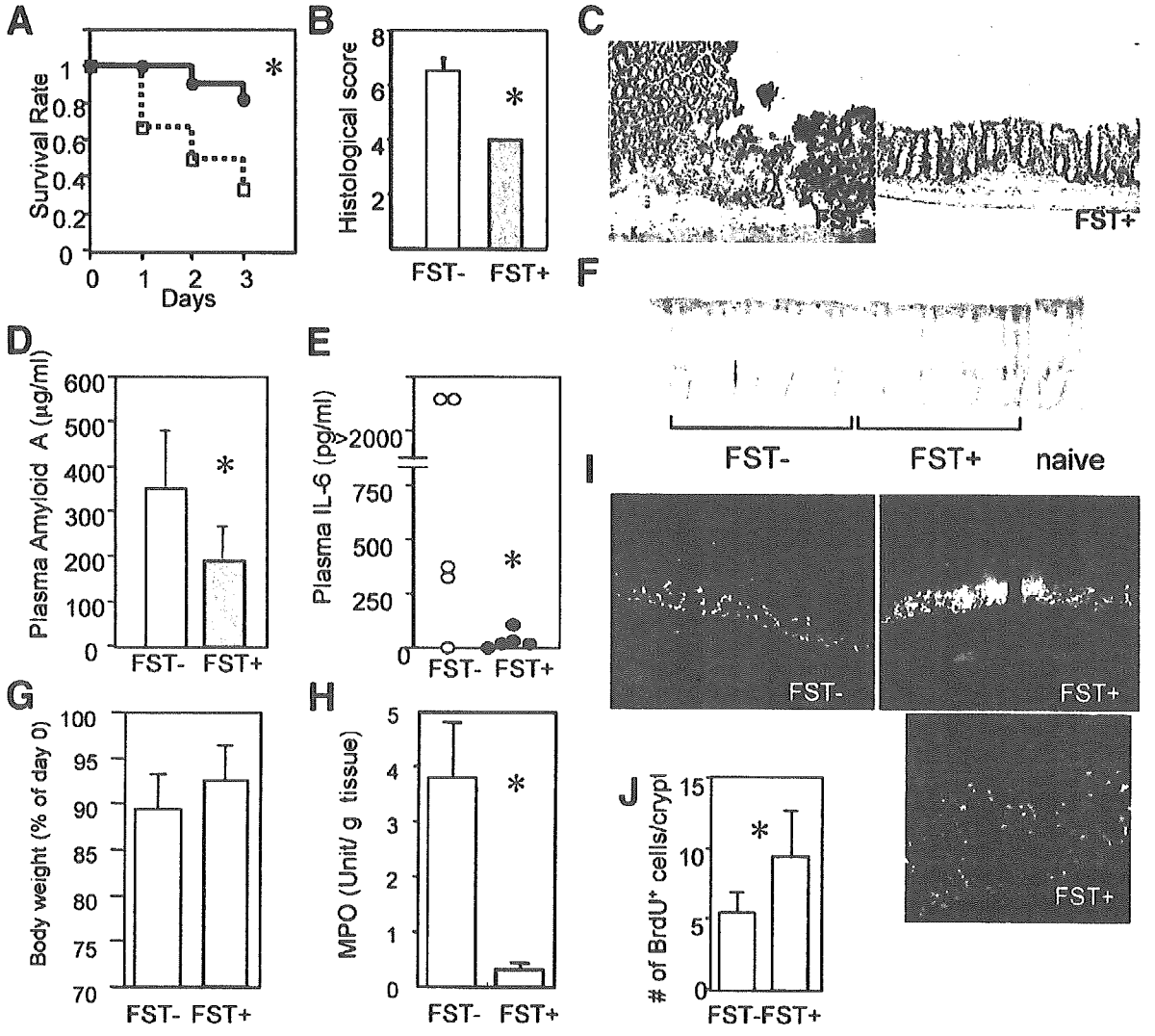

Figure 3. Successful treatment of TNBS colitis with follistatin. (*A*) The survival rate of mice 3 days after administration of TNBS (high dose, 60 μg/g of body weight). *Solid circles* indicate the mouse group pretreated with follistatin (n = 11), and *open squares* indicate the control group (n = 12). (*B*) Histologic scores for mice at day 3 following administration of TNBS (medium dose, 48 μg/g). Each group included 5 mice. One animal in the control group died on day 1. FST-, control group; FST+, follistatin-treated group. (*C*) Histologic features of the colon from mice pretreated (right) or not (left) with follistatin. The colon was removed 3 days after the administration of TNBS (48 μg/g). (*D* and *E*) Levels of amyloid A (*D*) and (*E*) plasma IL-6 were determined 24 hours after administration of TNBS (60 μg/g). Each group included 5 mice. (*F*) Plasma obtained from mice 24 hours after administration of TNBS (60 μg/g). (*G*) Body weight changes on day 3 after TNBS enema (48 μg/g) of follistatin-treated mice (n = 10) and control mice (n = 9). (*H*) Low MPO activity was seen in the colon of follistatin-treated mice. Colonic tissue was obtained 24 hours after administration of TNBS (60 μg/g). (*I*) Typical results of staining with anti-BrdU Ab of colon sections from mice pretreated with follistatin (right) or nontreated (left). The colons were taken 3 days after the administration of TNBS (48 μg/g). To show that the majority of the $BrdU^+$ cells were epithelial cells, sections were counterstained with DAPI (*blue*), and $BrdU^+$ cells are shown in *purple* at high-power magnification in the lower right panel. (*J*) Numbers of $BrdU^+$ cells in the colon. Twenty crypts in the midcolon from each of 5 mice from the groups shown in panel *G* were examined. Values are shown as mean with 1 standard deviation. *The difference between the control group (FST-) and the follistatin-pretreated group (FST+) was statistically significant ($P < .05$).

(Tel-Test, Inc., Friendswood, TX). Complementary DNA was synthesized from RNA by reverse transcription (RT). The PCR primers for murine GAPDH used were 5′-AGCCAA-ACGGGTCATCATCTC and 5′-TGCCTGCTTCACCAC-CTTCTT; those for activin βA, 5′-TGCTGCACTTGAA-GAAGAGA-CCC and 5′-TGGTCCTGGTTCTGTTAGC-CTTG; those for activin βB, 5′-ATGGACTTTCGGCTCAT-CGG and 5′-CACGATCATGTTGGGCACATC; and those for follistatin, 5′- CCTACTGTGTGACCTGTAA-TC and 5′-CTCCTCTTCCTCCGTTTCTTC. The step-cycle program was set for denaturing at 95°C for 45 seconds, annealing at 60°C for 45 seconds, and extension at 72°C for 45 seconds for a total of 40 cycles. Expression of mRNA was assessed by quantitative PCR using a SYBR Green PCR Master Mix

(Applied Biosystems, Warrington, United Kingdom) and ABI PRISM 7700 Sequence Detector (Applied Biosystems). Quantification of mRNA for IFN-γ was performed by using ABI Taqman probes (Applied Biosystems). The PCR primers for IFN-γ were 5′-TGATCCTTTGGACCCTCTGA and 5′-GCAAAGCCAGATGCAGTGT, and the Taqman probe was 5′-CCTCCTGCGGCCTAGCTCTGAGAC. Threshold cycle numbers (Ct) were determined with Sequence Detector Software (version 1.7; Applied Biosystems) and transformed by using the ΔCt/ΔΔCt method as described by the manufacturer, with GAPDH used as the calibrator gene.

Statistics

The results were compared by the Mann–Whitney test using the Statview II statistical program (Abacus Concepts, Berkeley, CA) adapted for the Macintosh computer. Differences in survival rate were tested by the Kaplan–Meier test. Changes in body weight were compared by use of the Wilcoxon matched-pair signed-rank test.

Results

Activin Is Up-regulated During the Acute Phase of TNBS Colitis

We first investigated the expression of activins and follistatin in the inflamed murine colon by using the TNBS colitis model. In this model, acute erosive lesions with infiltrating leukocytes were observed on days 1–3. Activin βA mRNA was detected in the colon of normal mice. Although the signal was not a strong one, epithelial cells and LPMC contained activin βA mRNA (Figure 1*A* and 1*C*). In contrast, one day after the induction of colitis, activin βA transcripts were remarkably up-regulated in epithelial cells in the lower crypts, in the infiltrating cells, and also in the endothelial cells (Figure 1*B* and *D*).

When the time course for mRNA expression of activin βA, activin βB, and follistatin in the colon was assessed by quantitative RT-PCR, up-regulation of activin βA was evident at day 1 (Figure 2). Follistatin mRNA was also increased at day 1 but to a lesser degree than activin βA mRNA (Figure 2*A*). Plasma levels of activin A peaked at day 3 and decreased by day 7 (Figure 2*B*). These results suggest that excess activin A was produced during the acute phase of TNBS colitis. For further evaluation of the fraction of the infiltrating cells that was responsible for the inflammation-related synthesis of activins, we separated total colonic LPMCs into adherent cells, which were mostly $CD11b^+$ cells (>90%), and nonadherent, floating cells, which were mainly lymphocytes.

Messenger RNA expression for activins βA and βB induced by inflammation took place mainly in the adherent LPMC fraction (Figure 2*C*). Activin A was detected by ELISA in the supernatants of $CD3^+$ T-cell and $B220^+$ B-cell fractions; however, up-regulation of activin A release after induction of TNBS colitis was evident only in the adherent cell fraction (Figure 2*D*). It was also clear that follistatin mRNA levels did not change at this time point in either fraction of LPMCs (Figure 2*C*). This result suggests that the increased levels of activins in the colon may not have been neutralized by follistatin.

Follistatin Prevents Acute Colitis

We next tested the effects of follistatin for its ability to neutralize activins during the acute phase of TNBS colitis. A single administration of follistatin 30 minutes before the induction of colitis significantly improved the survival rate of the mice at day 3 (Figure 3*A*). Histologic scores were lower in the group treated with follistatin (Figure 3*B*). In TNBS colitis, focal ulcers were prominent at day 3; however, mice given follistatin showed a lower frequency of these erosive lesions than the control group, although mild edema and evidence of cell infiltration were observed (Figure 3*C*). Plasma amyloid A and IL-6 levels were also significantly lower in the mouse group treated with follistatin than in the control, nontreated group (Figure 3*D* and *E*). Plasma obtained from mice within 24 hours after intracolonic administration of TNBS showed the characteristic yellow color derived from the trinitrophenyl (TNP) residue; however, the plasma from TNBS-treated mice given follistatin was not colored by the TNBS (Figure 3*F*). When body weight was measured on day 3 after a medium dose of TNBS had been given, the follistatin-treated group showed less weight loss than the control group, although this difference did not reach statistical significance (Figure 3*G*). MPO activity in the colonic tissue, which reflects the accumulation of neutrophils, was much lower in the follistatin-treated than in the control group, and coincided with less ulcer formation in the follistatin-treated group (Figure 3*H*). Of note, enhancement of epithelial cell proliferation was seen in the mouse group treated with follistatin (Figure 3*I* and *J*).

Rapid provision of new epithelial cells by accelerated division may be one of the mechanisms for the anti-inflammatory effects of follistatin. In the acute phase of TNBS colitis, damage to the colonic mucosa resulted in bacteremia, which is likely the major reason for the early death seen in these mice. We speculate that follistatin accelerates prompt epithelial cell regeneration in the colon and thus improves the barrier function of the colonic mucosa.